Article

Current Biology

Cortical cellular encoding of thermotactile integration

Graphical abstract

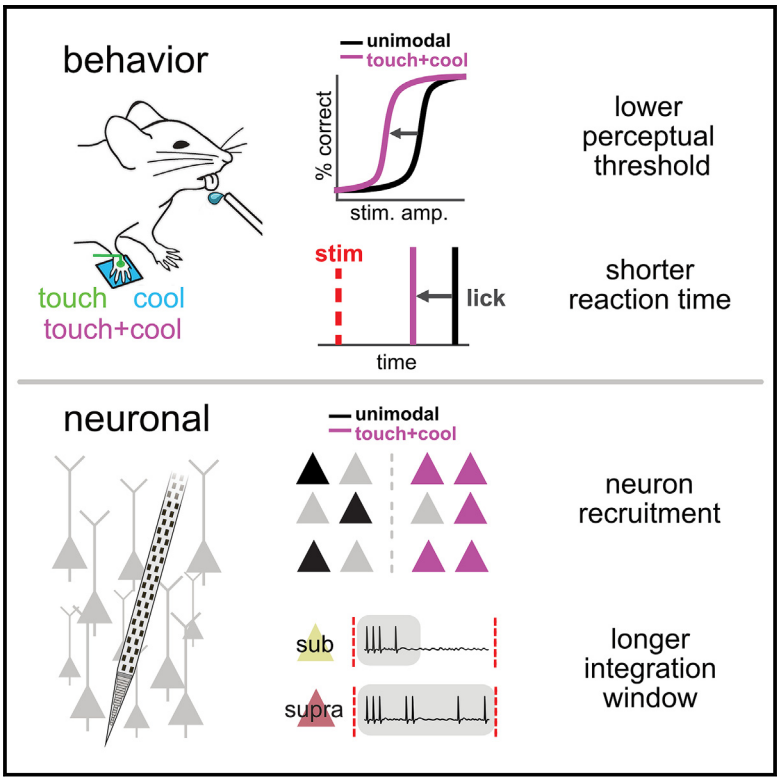

Highlights

- Mouse thermotactile perception and cortical thermotactile integration
- Mice show enhanced perception to bimodal compared with unimodal stimuli
- Extracellular electrophysiological recordings from forelimb S1
- Identification of key response features of S1 neurons during thermotactile integration

Authors

Philipp Schnepel, Ricardo Paricio-Montesinos, Ivan Ezquerra-Romano, Patrick Haggard, James F.A. Poulet

Correspondence

james.poulet@mdc-berlin.de

In brief

Perception involves the integration of multiple modalities of sensory information. Schnepel et al. report that mice show enhanced perception to bimodal, thermotactile stimuli compared with unimodal touch or cool. Extracellular recordings of S1 neurons identify key thermotactile response features by comparing unimodal with bimodal responses.

Schnepel et al., 2024, Current Biology *34*, 1–13
April 22, 2024
https://doi.org/10.1016/j.cub.2024.03.018

CellPress

Current Biology

CellPress
OPEN ACCESS

Article

Cortical cellular encoding of thermotactile integration

Philipp Schnepel,[1,2] Ricardo Paricio-Montesinos,[1,2] Ivan Ezquerra-Romano,[1,2,3] Patrick Haggard,[3] and James F.A. Poulet[1,2,4,*]

[1]Max-Delbrück Center for Molecular Medicine in the Helmholtz Association (MDC), Berlin-Buch, Robert-Rössle-Strasse 10, 13125 Berlin, Germany

[2]Neuroscience Research Center, Charité-Universitätsmedizin Berlin, Charitéplatz 1, 10117 Berlin, Germany

[3]Institute of Cognitive Neuroscience, University College London (UCL), London WC1N 3AZ, UK

[4]Lead contact

*Correspondence: james.poulet@mdc-berlin.de

https://doi.org/10.1016/j.cub.2024.03.018

SUMMARY

Recent evidence suggests that primary sensory cortical regions play a role in the integration of information from multiple sensory modalities. How primary cortical neurons integrate different sources of sensory information is unclear, partly because non-primary sensory input to a cortical sensory region is often weak or modulatory. To address this question, we take advantage of the robust representation of thermal (cooling) and tactile stimuli in mouse forelimb primary somatosensory cortex (fS1). Using a thermotactile detection task, we show that the perception of threshold-level cool or tactile information is enhanced when they are presented simultaneously, compared with presentation alone. To investigate the cortical cellular correlates of thermotactile integration, we performed *in vivo* extracellular recordings from fS1 in awake resting and anesthetized mice during unimodal and bimodal stimulation of the forepaw. Unimodal stimulation evoked thermal- or tactile- specific excitatory and inhibitory responses of fS1 neurons. The most prominent features of combined thermotactile stimulation are the recruitment of unimodally silent fS1 neurons, non-linear integration features, and response dynamics that favor longer response durations with additional spikes. Together, we identify quantitative and qualitative changes in cortical encoding that may underlie the improvement in perception of thermotactile surfaces during haptic exploration.

INTRODUCTION

A fundamental function of the brain is the integration of different streams of sensory input. Quantitative behavioral testing in humans and animal models has shown that multisensory integration enhances perceptual performance.[1–10] Most of our understanding of the neural encoding of multisensory stimuli, such as the principles of "inverse effectiveness" or spatial and temporal congruency, comes from studies in the superior colliculus.[11–13] In contrast, the neocortex plays a major role in multisensory perception,[7] but less is known about the rules of multisensory integration in cortical circuits.

Cortical multisensory integration has been thought of as a hierarchical process, with unimodal, primary cortices providing converging input to higher-order regions for integration with other modalities.[14–18] Recent work, however, has suggested that primary cortical sensory areas also play a role in multisensory integration.[4,19–25] However, the responses of primary cortical sensory areas to other modalities are typically sparse and weak[22,26] and have been thought of as modulatory or even mere artifacts of behaviorally generated activity.[27] To address the cellular representation of cortical multisensory integration, we take advantage of the strong representation of tactile and cool information in mouse primary forelimb somatosensory cortex (fS1).[28,29] The thermotactile system has been less studied than other sensory pathways, but it is a highly relevant system to examine sensory integration. Thermal and tactile information are constantly integrated during haptic exploration of object surfaces, and intriguingly, somatosensory illusions hint at a profound interaction between thermal and tactile pathways. For example, the lack of hygroreceptors in primary somatosensory afferent neurons indicates that our sense of wetness is created centrally by the integration of thermal with tactile information.[30] Furthermore, Weber's "Thaler illusion" shows that colder objects appear heavier than those of a neutral temperature.[31] In "thermal referral," the thermal component of a combined thermotactile sensation spreads to an adjacent skin region exposed to thermally neutral touch.[32–34]

Prior work addressing multisensory integration has focused on sensory information detected by different sense organs, especially audio-visual integration. Despite both being part of the somatosensory system and detected by the same sense organ, we view thermal and tactile information as different sensory modalities. Partly because they are transduced by dedicated peripheral sensory afferent neurons expressing distinct ion channel receptors, but also, unlike visual sub-modalities, which arise from detection of electromagnetic radiation by the retina, thermal and mechanosensory stimuli are transmitted as different forms of physical energies (thermal energy vs. mechanical

Please cite this article in press as: Schnepel et al., Cortical cellular encoding of thermotactile integration, Current Biology (2024), https://doi.org/10.1016/j.cub.2024.03.018

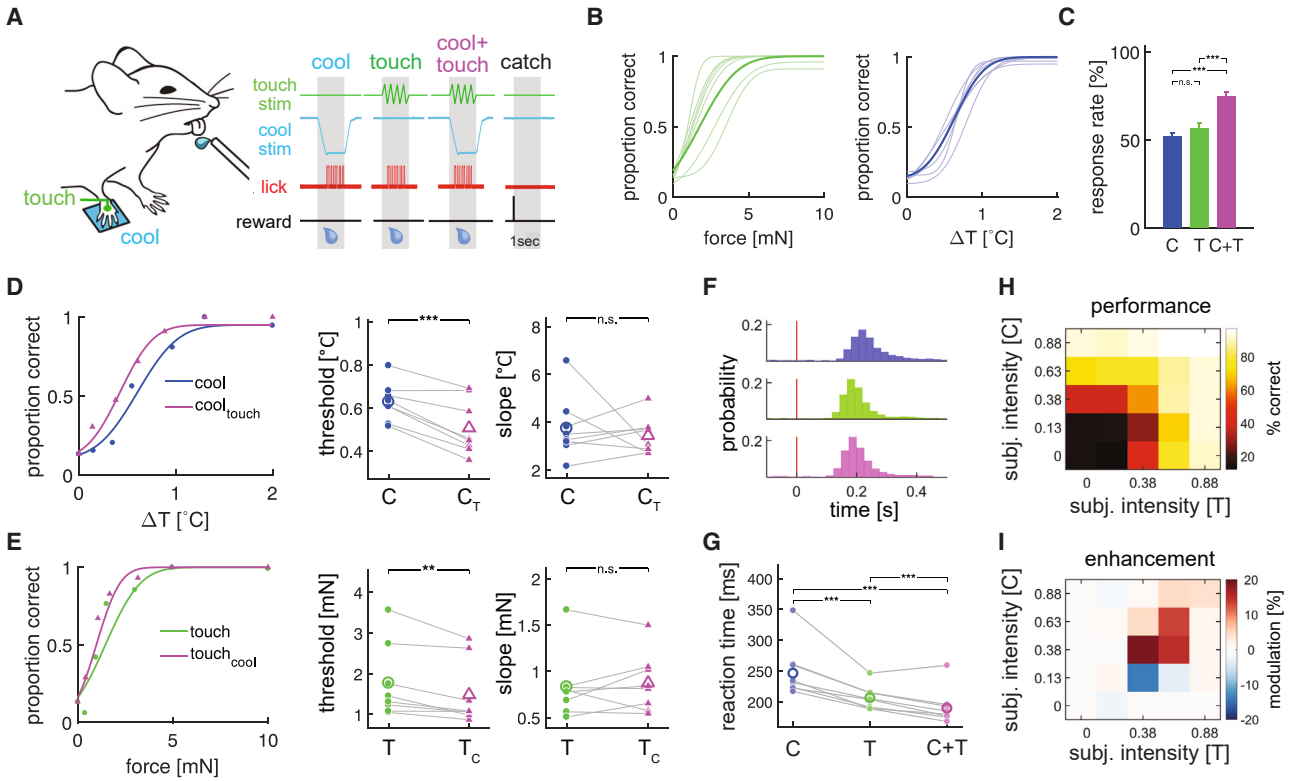

Figure 1. Mice exhibit performance enhancement in a thermotactile detection task

(A) Left: behavioral setup. Right: Go/No-go task design with rewarded (stimulus) and unrewarded (catch) trials.

(B) Psychometric curves for touch and cool stimuli for n = 8 mice (average in bold).

(C) Average response rates across all animals; error bars show SEM.

(D) Left: psychometric curves for cool (blue) and cool + subthreshold touch (magenta) for an example animal. Right: thresholds and slopes from the psychometric curves for each animal (open symbols show mean).

(E) Same as in (D) but for touch (green) and touch + subthreshold cool (magenta).

(F) Distributions of first lick times for each condition.

(G) First lick latency (reaction time) for supra-threshold cool, touch, and cool + touch stimuli.

(H) Normalized % correct response rates for all stimulus combinations (subjective intensity), averaged across all animals.

(I) The difference between the bimodal performance and the "best" unimodal performance (modulation in %: (Bi-Uni_{max})/Uni_{max})) from (H) reveals that the strongest enhancement happens around threshold. Axis tick labels denote bin centers.

ANOVA (C and G) and paired t test (D and E): *p < 0.05, **p < 0.01, and ***p < 0.001.

See also Figure S1.

pressure). Overall, the thermotactile system offers a unique opportunity to examine how different modalities of sensory input are integrated in the cortex. However, whether mice show changes in perceptual performance during thermotactile processing and how fS1 neurons integrate cool and touch inputs have not been examined. Here, we address these questions in the mouse forepaw system.

RESULTS

The addition of a second modality enhances cool and touch detection rates and lowers perceptual threshold

Mice use their forepaws with great dexterity during foraging, food consumption, haptic exploration, and social interactions. Like human hands, the mouse forepaw is extremely sensitive to tactile and thermal stimuli and can detect milli-Newton scale forces and temperature changes of <1°C.[29,35,36] Inspired by a mouse audio-visual detection task,[37] we designed a thermotactile Go/No-Go detection task to assess the psychophysical abilities of mice to detect unimodal and bimodal thermotactile stimuli (Figure 1A). We hypothesized that combining cool with touch stimuli would enhance perceptual performance.

Head-restrained, paw-tethered mice were trained to report the presence of a cool or touch stimulus by licking a waterspout. Once they reached a stable performance level, we generated session-by-session psychometric curves for cool and touch stimuli with an adaptive staircase procedure (Figures 1B and S1A) and pseudo-randomized the delivery of bimodal (cool and touch, C + T) and unimodal (cool, C or touch, T) stimuli (STAR Methods). For each mouse, perceptual thresholds were combined across 5–11 testing sessions to increase statistical validity (average 1,959 trials per mouse, range: 1,138–2,944). Average unimodal perceptual thresholds were 0.63°C ± 0.09°C for cool and 1.77 ± 0.9 mN for touch stimuli (n = 8 mice).

Please cite this article in press as: Schnepel et al., Cortical cellular encoding of thermotactile integration, Current Biology (2024), https://doi.org/10.1016/j.cub.2024.03.018

CellPress
OPEN ACCESS

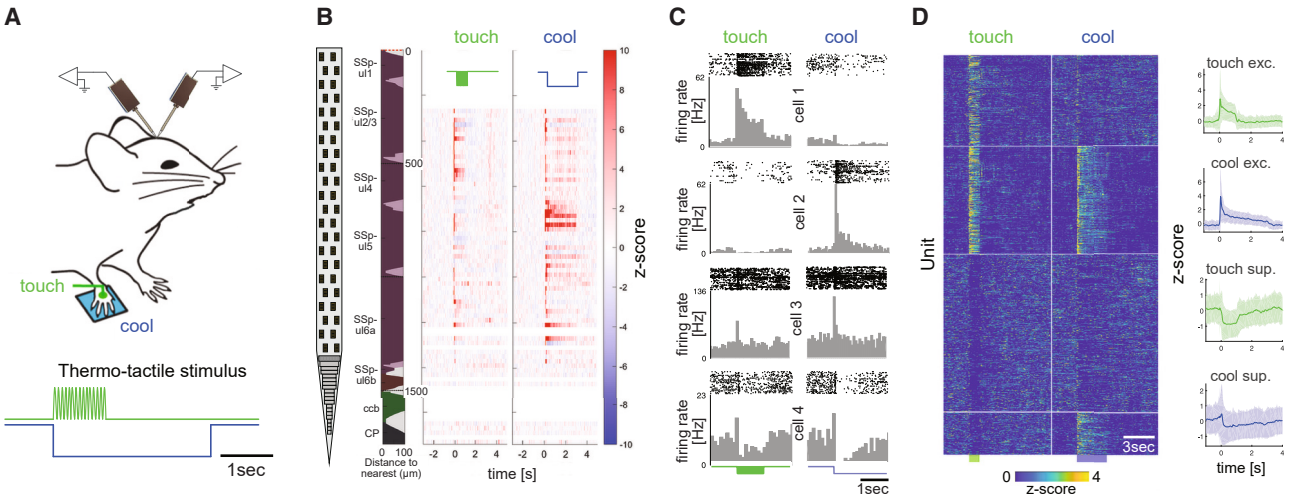

Figure 2. Extracellular recordings of touch and cool responses in awake mouse fS1

(A) Recording setup: head-restrained, awake mice receive tactile (60 Hz, 1 s) and cool (3 s) stimuli to their right forepaw during extracellular recordings with up to two neuropixel probes.

(B) Example recording showing the reconstructed location of probe sites across cortical layers (SHARP-track) and *Z*-scored firing rate responses across the probe shank for touch and cool stimulation. SSp-ul, primary somatosensory area upper limb; ccb, corpus callosum body; and CP, caudoputamen.

(C) Responses of four example units to touch and cool.

(D) Left: hierarchical clustering of maximum unimodal stimulus (20 mN/−8°C) responses of all units (n = 1,149 units). Each row shows the concatenated, *Z*-scored response to maximum touch (left) and cool (right) stimulation for one unit. Units are arranged by cluster to reveal the overlap between touch and cool representations. Right: *Z*-scored, averaged response of touch/cool excited and touch/cool suppressed (including unresponsive) clusters (shaded area, ±2 SD).

See also Figure S3.

Hallmarks of multisensory behavioral enhancement in other systems are lower response latencies and higher stimulus detection rates, compared with unimodal stimuli. Consistent with this, mice showed higher detection rates to bimodal than unimodal stimuli (Figure 1C; C = 52%, T = 57%, and C + T = 75%; with p = 0.35 for C vs. T, p = 3.8 × 10^{-6} for C vs. C + T, and p = 9.4 × 10^{-5} for T vs. C + T). We went on to further assess perceptual performance by fitting psychometric functions to the detection rates of different amplitude unimodal and bimodal stimuli (left graphs, Figures 1D and 1E) and compared the threshold for each mouse. Both cool and touch detection thresholds were decreased when adding subthreshold stimuli of the second modality (C, 0.63°C ± 0.09°C vs. C_T, 0.51°C ± 0.13°C, p = 9.3 × 10^{-4}; T, 2.20 ± 1.0 mN vs. T_C, 1.49 ± 0.79 mN, p = 0.009; Figures 1D and 1E), suggesting increased multisensory performance. Moreover, while mice responded to cool with longer latency than to touch (C, 246.1 ± 2.4 ms vs. T, 206.3 ± 2.1 ms, p = 1.0 × 10^{-34}), they responded to thermotactile stimuli with shorter latency than to cool or touch stimuli (C + T 189.5 ± 1.7 ms, C + T vs. C, p = 8.4 × 10^{-68}, C + T vs. T, p = 9.9 × 10^{-9}; Figures 1F, 1G, and S1B).

Detection performance can also be evaluated by the steepness of the slope of the psychometric function around threshold, with a steeper slope indicating higher detection reliability and increased accuracy. We observed no overall difference between unimodal and bimodal conditions of the slope (C, 3.74°C ± 1.31°C vs. C_T, 3.44°C ± 0.77°C, p = 0.6 and T: 0.83 ± 0.36 mN vs. T_C: 0.87 ± 0.32 mN, p = 0.54; right graphs, Figures 1D and 1E), indicating that there was no significant improvement in detection reliability to thermotactile stimuli.

To quantify thermotactile enhancement, we normalized the stimulus space and calculated the proportion of correct responses (Figure 1H), as well as the difference between the largest unimodal and bimodal response rate (Figure 1I). These plots show that the degree of thermotactile enhancement is largest around threshold (0.5) for both modalities. Together, our data show that mice exhibit enhanced performance during the thermotactile detection task.

Unimodal cool and touch stimuli excite and inhibit fS1 neurons

fS1 neurons respond to cool and/or touch,[28,29] but the degree of response overlap has not been characterized at the population level. To address this and to attempt identifying neural correlates of enhanced thermotactile perceptual performance (Figure 1), we performed extracellular recordings from fS1 neurons in awake mice (Figures 2A and 2B). To control for the effects of arousal and movement, we also performed recordings in isoflurane anesthetized mice (Figure S2).

Recordings were targeted to left fS1, using intrinsic signal optical imaging, and the recording sites were confirmed post hoc using DiI staining of the probe tract (Figure S3). We presented cool, touch, or simultaneous cool + touch stimuli to their right forepaw at different amplitudes (5, 10, and 20 mN for touch and −1°C, −2°C, −4°C, and −8°C from a baseline of 32°C for cool). We first examined single-unit responses to unimodal stimuli (Figure 2C) and found different combinations of responses that were either excitatory or inhibitory/unresponsive. To visualize the overlap of these response classes, we used hierarchical clustering as an unbiased method to categorize units into

Please cite this article in press as: Schnepel et al., Cortical cellular encoding of thermotactile integration, Current Biology (2024), https://doi.org/10.1016/j.cub.2024.03.018

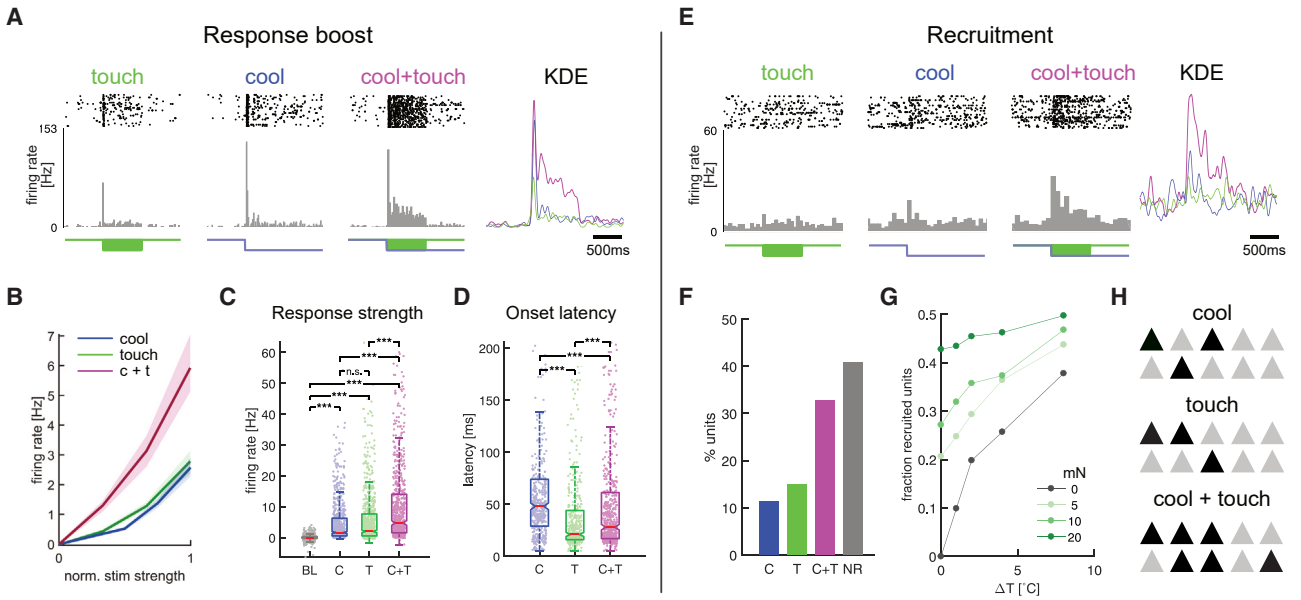

Figure 3. Bimodal stimulation boosts fS1responses and recruits additional neurons

(A) An example unit response to touch, cool, and cool + touch stimulation. Kernel density estimate (KDE) comparison shows increased response to cool + touch.

(B) Average firing rate of all responsive units to increasing stimulus intensity (normalized) for touch (5, 10, and 20 mN), cool (−1°C, −2°C, −4°C, and −8°C), and cool + touch stimulation.

(C) Maximum, baseline-corrected response strength of all responsive units for each stimulus condition; baseline (BL) firing rate is added for comparison. Significant differences in the medians were determined by multiple comparison testing (Kruskal-Wallis test, *p < 0.05, **p < 0.01, and ***p < 0.001).

(D) Same as in (C) but for onset latency.

(E) Responses of one example unit to touch, cool, and cool + touch stimulation. KDE comparison shows recruitment in the cool + touch condition.

(F) Fractions of responsive (C, T, and C + T) and unresponsive (NR) single units at maximum intensity stimulation.

(G) The fraction of recruited units as a function of stimulus intensity.

(H) Cartoon schematic showing that touch or cool stimulation recruits a subset of neurons that responds to the respective single modality or to both (black/gray triangles: active/inactive neurons). In addition, bimodal stimulation recruits unimodally "silent" neurons, such as that shown at bottom right.

See also Figure S2.

response profiles (excited or inhibited/unresponsive for C or T stimuli, i.e., 2 × 2 = max. 4 possible clusters). Clustering showed that 41% of recorded neurons were unresponsive or inhibited to unimodal stimulation, 32.7% neurons showed excitatory responses to both cool and touch, and 11.3% were excited by cool only and 15.1% to touch only. Of cool responsive neurons, 33% were unresponsive or inhibited by touch. Of the touch responsive neurons, 45% were unresponsive or inhibited by cool (Figure 2D). These results show that fS1 neurons exhibit varying levels of modality-specific excitation and inhibition to thermotactile stimuli.

Thermotactile stimulation boosts cortical responsiveness and recruits silent neurons

Prior work in different systems has suggested that neuronal responses to bimodal stimuli are amplified, compared with responses to unimodal stimuli.[7] To examine whether this was the case in the thermotactile system, we investigated the maximum response amplitude of fS1 neurons that were significantly excited by any stimulus type (e.g., Figure 3A). We compared the maximum response amplitude to unimodal cool with maximum response to unimodal touch and to the maximum response to bimodal cool + touch across the entire population of responsive units at a range of stimulus amplitudes (Figure 3B). The median excitatory response strength to unimodal cool and touch stimuli is comparable (C, 1.63 Hz; T, 2.00 Hz), whereas there is a significantly stronger response to bimodal cool + touch stimuli (C + T, 4.75 Hz; Figures 3A–3C). Similar to the psychophysical performance, the median fS1 neuron response latency to cool was delayed, compared with touch (C, 48 ms and T, 21 ms; Figure 3D), but was longer than the cool + touch response latency (28 ms). Although anesthesia caused an overall reduction in firing rates and a reduced cool response relative to touch, similar to awake data, the response strength was higher to bimodal compared with unimodal stimuli, and the bimodal response latency was in between the unimodal cool and touch response latencies (Figures S2A and S2B). Altogether, this indicates that these results are not due to changes in arousal level or movement. Overall, bimodal thermotactile stimulation drives the fS1 circuit more effectively than unimodal cool or touch.

Although most responsive neurons were excited by both modalities (e.g., Figure 3A), some neurons could exhibit excitation for one modality and inhibition for the other (Figures 2C and 2D). We reasoned that unimodally silent or inhibited neurons could be unmasked by the combined thermotactile drive and thus be recruited to increase the overall number of cells representing a thermotactile stimulus in fS1 (e.g., unit in Figure 3E). To test this and to quantify the population size, we next examined the dependence of recruitment on stimulus amplitude and calculated the fraction of responsive units at increasing stimulus

Please cite this article in press as: Schnepel et al., Cortical cellular encoding of thermotactile integration, Current Biology (2024), https://doi.org/10.1016/j.cub.2024.03.018

intensities during unimodal and bimodal stimulation (Figure 3G). As expected, the number of recruited neurons increases with increasing unimodal cool amplitude (gray line). When including a simultaneous touch stimulus (green lines), the number of recruited neurons increases (vertical shift in the green lines at a given thermal stimulus amplitude). This increase plateaus toward the maximum touch and cool stimulus strengths, likely due to the network operating at the upper end of its dynamic range (a "ceiling effect"). Thus, at low stimulus intensities, adding a second modality results in relatively more units being recruited than at higher stimulus intensities (i.e., larger difference between the green lines at lower compared with higher cool amplitudes). These relationships were also observed in anesthetized recordings and were therefore not due to arousal or movement-related activity (Figure S2D). These data suggest that the recruitment of unimodally silent or inhibited neurons is a major feature of thermotactile stimulus representation in fS1 (Figure 3H).

Non-linear processing in fS1 during thermotactile integration

Are multisensory neural responses predictable from their responses to unimodal stimuli? A widely used metric to address this key question is "response additivity." Classically, the response of a unit to bimodal stimulation is compared with the arithmetic sum of the corresponding unimodal responses. Units are then categorized as supra-additive, additive, or sub-additive (Figure 4A; STAR Methods). To investigate these sub-populations in our dataset, we used a standard metric termed "multisensory index" (MSI).[11] The MSI is a normalized quantification of multimodal enhancement/suppression (STAR Methods). We observed examples of supra-additive (Figure 4B, top; MSI > 0), additive (Figure 4B, middle; MSI ~0), and sub-additive units (Figure 4B, bottom; MSI < 0) during thermotactile stimulation. The majority of fS1 units were classified as supra- or sub-additive (49.7% and 39.3%, respectively) and only a smaller fraction as additive (11.0%; Figure S4A). Plotting the thermotactile responses against the corresponding sum of both unimodal responses (Figure 4E) showed a clear separation from the isocline for the supra- and sub-additive populations, confirming that most thermotactile responses in fS1 are non-linear and not predictable from their unimodal response.

Classic studies in the superior colliculus have proposed a second rule to boost low-saliency stimuli and improve signal representation termed inverse effectiveness. This rule suggests that a neuron's multisensory enhancement is inversely proportional to the unimodal response strength (Figure 4C and example cell in Figure 4D). The focus of multisensory integration analysis is normally on those neurons showing enhancement of multisensory responses as compared with their unimodal responses. However, we observed a significant proportion of neurons with sub-additive effects. In order to simplify the comparison of inverse effectiveness between the different populations, we plotted our data in a semi-log space and fitted separate regressions for each functional sub-population (Figures 4F and 4G). While supra-additive units showed weak, positive inverse effectiveness ($r = -0.30$, $p = 7.7 \times 10^{-5}$), sub-additive and additive units exhibited negative inverse effectiveness ($r = 0.60$, $p = 1.2 \times 10^{-28}$ and $r = 0.24$, $p = 0.05$, respectively), i.e., an increase of thermotactile suppression with decreasing unimodal response strength. These correlations were also observed when plotting the data as an absolute modulation against the arithmetic sum of the corresponding unimodal stimulus response (Figures S4D and S4E).

These results indicate that thermotactile units show the largest non-linearity in summation at low stimulus saliency levels, both for enhancement and suppression. This mirrors the findings from unit recruitment (Figure 3G) and the behavioral detection task (Figure 1I), where the largest changes are observed at low stimulus levels. Interestingly, although we observed similar effects of thermotactile additivity and the recruitment of units during thermotactile stimulation under isoflurane anesthesia, inverse effectiveness was only significant in the sub-additive population (Figures S2D–S2F). Our results highlight that a significant aspect of cortical thermotactile integration is the interplay between non-linear enhancement and suppression of neural responses.

Thermotactile responses in fS1 are prolonged and include additional action potentials

Non-linear changes of responses in bimodal integration are usually reflected by a quantitative change in the absolute number of action potentials (APs) during the stimulus period. However, a neuron's response can also be changed qualitatively by altering its temporal response dynamics. Cortical neuron responses to thermal stimuli have been described as either transient or sustained.[29] In agreement, we observed three major types of unimodal response dynamics: cells with an excitatory transient response (e.g., Figures 3A and 4B, top), cells with an excitatory sustained response (e.g., Figures 2C, top left, and 4B, middle), and cells whose response was suppressed/unresponsive (e.g., Figure 2C, bottom).

To investigate the relationship between response dynamics during thermotactile stimulation and additivity further, we applied hierarchical clustering to cool and touch responses separately in the sub-additive, supra-additive, and additive populations and expanded our initial clustering approach from 2 to 3 target clusters. This yielded clusters containing mostly transient, sustained, and suppressed/unresponsive units for touch, cool, and thermotactile groups (i.e., a total of $3 \times 3 = 9$ combinations; Figure S5A; STAR Methods). We next graphically ordered them by the thermotactile response dynamic (top, sustained; middle, transient; bottom, suppressed; Figures 5A and 5B). While the additive population did not show any significant differences in their temporal dynamics between unimodal and thermotactile stimulation (Figure S5B), both the supra- and sub-additive populations exhibited significant differences. In the sub-additive population, differences were most obvious in "suppressed" units (Figure 5A, e.g., cluster 9), suggesting a prominent role for synaptic inhibition. In contrast, the supra-additive population contained many units that were unmasked when both stimuli were presented together (Figure 5B, e.g., clusters 2 and 3). Strikingly, these clusters contained a large number of units with more sustained responses to thermotactile stimulation (Figure S4B), indicating that response prolongation could be a central aspect of thermotactile integration.

To examine this further, and to control for arousal, we compared response features from our awake and anesthetized datasets during cool + touch stimulation with experiments where

Please cite this article in press as: Schnepel et al., Cortical cellular encoding of thermotactile integration, Current Biology (2024), https://doi.org/10.1016/j.cub.2024.03.018

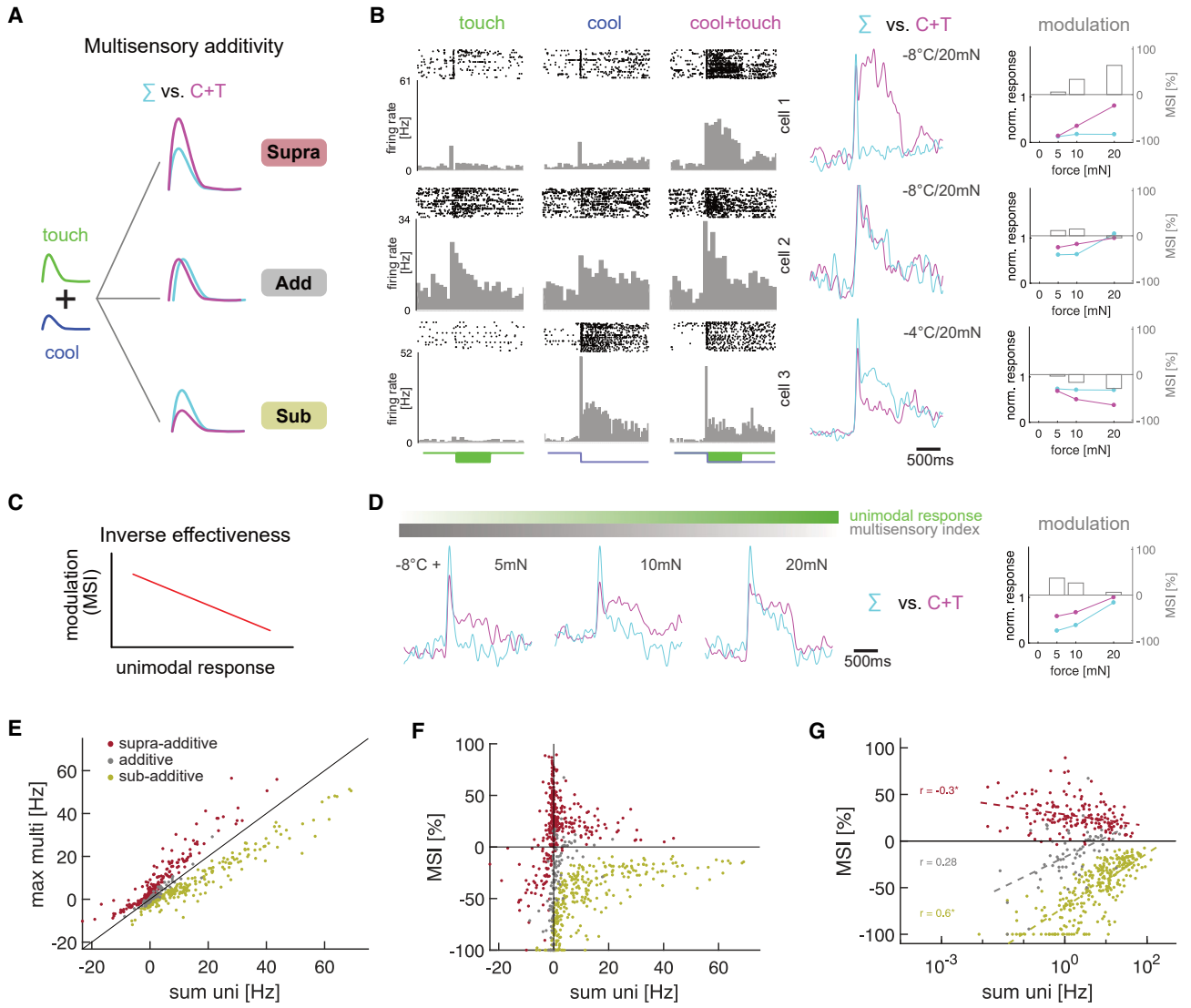

Figure 4. Additivity and inverse effectiveness during thermotactile integration

(A) Schematic showing possible combinations of responses to bimodal stimuli. Comparing the arithmetic combination of unimodal T and C responses (∑) to the bimodal (C + T) response allows the definition of additive (gray) and sub-/supra-additive (yellow, red) sub-populations of neurons.

(B) Example units illustrating additivity: supra-additive (top), additive (middle), and sub-additive (bottom). Each row shows (from left to right): raster/PSTH for T, C, and C + T stimulus; kernel density estimate (KDE) of the firing rate for ∑ vs. C + T (scale bars, 500 ms); normalized response strength for ∑ and C + T (left axis); and corresponding MSI (gray bars, right axis) for one temperature (the example's stimulus combination is marked next to the KDE plot, e.g., −4°C/20 mN).

(C) Schematic representation of the principle of inverse effectiveness.

(D) Example unit illustrating inverse effectiveness. The modulation strength (difference between KDE for ∑ and C + T, gray bar) decreases with increased intensity of one modality (tactile strength increase from left to right, green bar; cool is fixed at −8°C). This is summarized in the modulation plot.

(E) Maximum C + T response plotted against the arithmetic sum of the corresponding unimodal responses for the "best" stimulus combination (STAR Methods) of each unit.

(F) MSI plotted against the arithmetic sum of the corresponding unimodal stimulus responses for all units.

(G) Same as in (F) but on a semi-log scale. Linear regression reveals a significant negative correlation (i.e., inverse effectiveness) for the supra-additive population but a positive correlation for the additive and sub-additive populations.

See also Figures S2 and S4.

we used warm or light stimuli instead of cool, two modalities that are poorly represented in fS1. We first averaged and normalized the thermotactile responses in the sub-additive, supra-additive, and additive populations (Figures 6Ai–6Aiv). Visual inspection shows a more prolonged thermotactile response for the supra-additive neurons as compared with the sub-additive and additive populations. To quantify this, we calculated a "duration index" for each unit that compared the strength of the first and last 200 ms of the response (Figures 6Bi–6Biv and S6). We found that the distribution for supra-additive units was significantly shifted to the right, compared with sub-additive units, both in awake and anesthetized mice ($p = 4.7 \times 10^{-15}$ and

Please cite this article in press as: Schnepel et al., Cortical cellular encoding of thermotactile integration, Current Biology (2024), https://doi.org/10.1016/j.cub.2024.03.018

CellPress
OPEN ACCESS

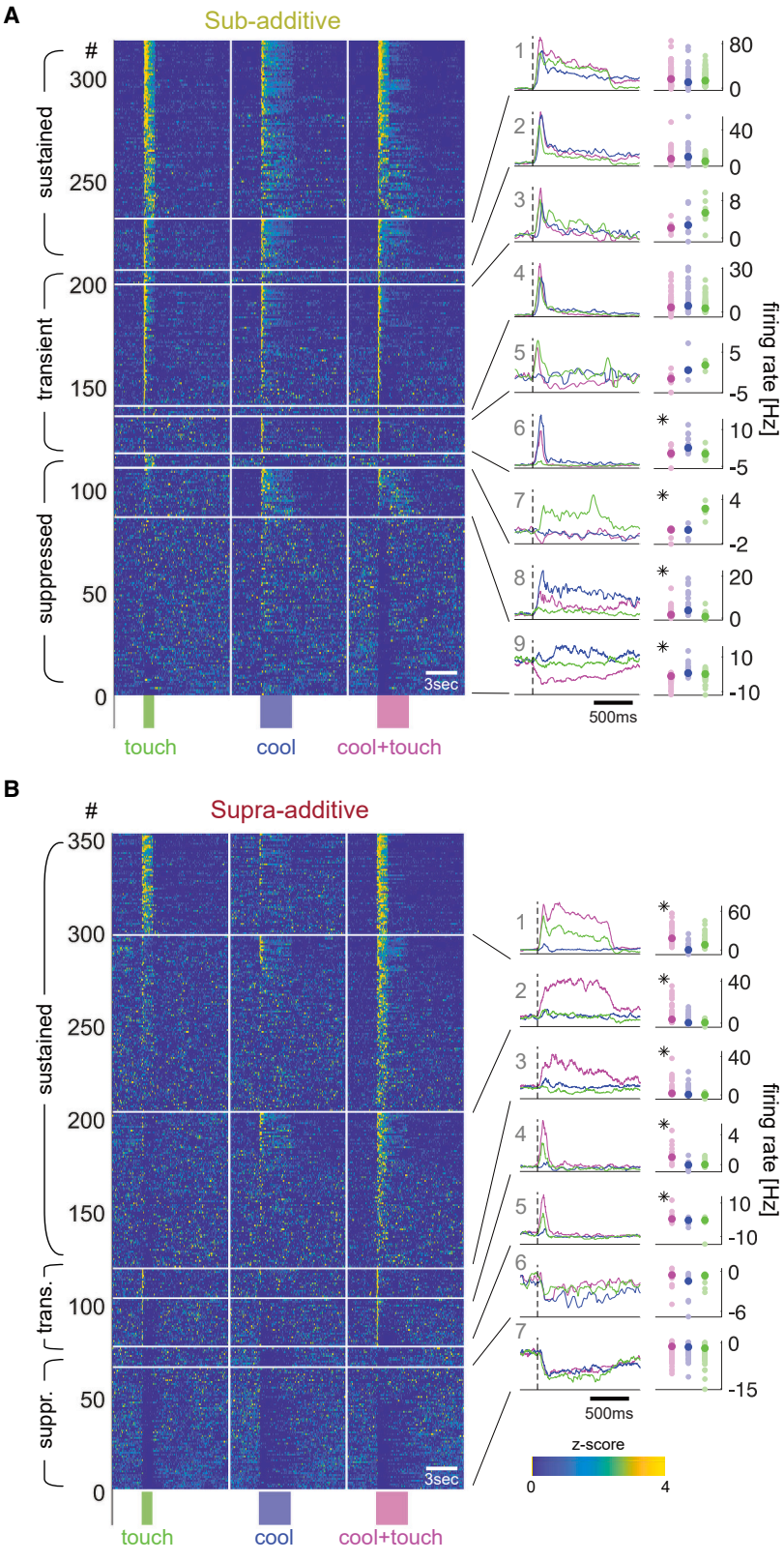

Figure 5. Temporal response dynamics of supra- and sub-additive units during thermotactile stimulation

(A) Hierarchical 3-by-3 clustering of the "best" C + T responses of the sub-additive sub-population. Each row shows the concatenated, *Z*-scored responses to T (left), C (middle), and C + T (right) stimulation for each unit. Clusters are ordered by temporal dynamics of the average C + T response (right panels). Within each cluster, units are ordered by peak C + T response strength. Right side panels show the average responses of each cluster and the average firing rate in the response window for each unit (darker symbols show average for T, C, and C + T, respectively). Asterisks denote significant differences between the bimodal and the best unimodal response ($p < 0.01$, Wilcoxon test).

(B) Same as in (A) but for the supra-additive sub-population.

See also Figure S5.

Please cite this article in press as: Schnepel et al., Cortical cellular encoding of thermotactile integration, Current Biology (2024), https://doi.org/10.1016/j.cub.2024.03.018

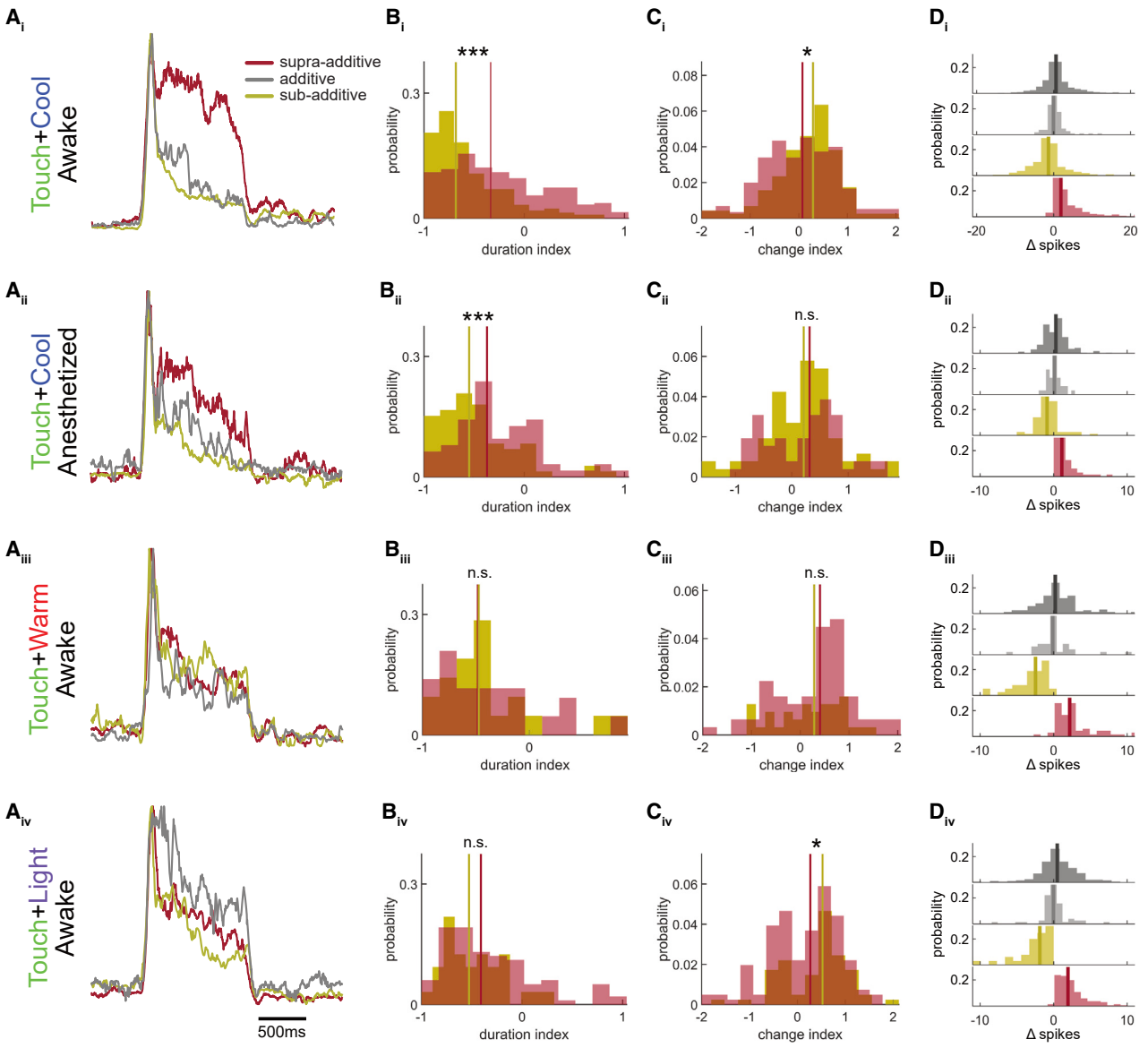

Figure 6. Supra-additive units strongly influence the population representation of thermotactile stimuli

(A) Normalized, average responses to bimodal stimulation. The supra-additive population exhibits more sustained response dynamics to bimodal cool + touch (Ai and Aii) than to warm + touch and light + touch stimuli (Aiii and Aiv).

(B) The duration index DI = ([L − E]/[L + E]) compares the first (E) and last (L) 200 ms of the response to generate a measure for sustained and transient responses. For C + T stimuli, the duration index of supra-additive units is shifted to the right, compared with sub-additive units (Bi and Bii), indicating a prolongation of the response. Lines denote medians of the respective distributions (Wilcoxon test from top to bottom: $p = 4.7 \times 10^{-15}$, $p = 8.0 \times 10^{-4}$, p = 0.13, and p = 0.88).

(C) Distribution of the "change index" for supra- and sub-additive populations. For each unit, the DI for each stimulus type (T, C, and C + T) is calculated separately, and the largest difference between the unimodal and bimodal stimulus response is taken as a measure of how much and in which direction the temporal dynamics change between conditions (0, similar temporal dynamics; +2, responses become more transient; −2, responses become more sustained; Wilcoxon test from top to bottom: p = 0.0026, p = 0.75, p = 0.44, and p = 0.04).

(D) Distributions of the difference in number of APs comparing responses to bimodal and the strongest unimodal stimuli for all units, separated by sub-population (top: combined distribution, dark gray). Vertical lines show medians.

See also Figure S6.

$p = 8.0 \times 10^{-4}$, respectively), but not in warm/light controls. This confirmed that a longer response duration is a specific feature of the integration of thermotactile information. Additionally, we calculated a "change index" by comparing the duration of the thermotactile with the longest unimodal responses within each unit (Figures 6Ci–6Civ). This analysis shows that supra-additive units' responses became more prolonged (i.e., a more negative index value) with thermotactile stimulation, compared with sub-additive units (p = 0.0026). This was not observed in anesthetized mice and in mice presented with touch + warm stimuli (p = 0.75

Please cite this article in press as: Schnepel et al., Cortical cellular encoding of thermotactile integration, Current Biology (2024), https://doi.org/10.1016/j.cub.2024.03.018

and p = 0.44, respectively, rows ii–iii), while responses to touch + light showed a modest effect of prolongation (p = 0.04, row iv). This indicates that response prolongation in fS1 is a specific feature of cool/touch integration.

Another central aspect of a cortical sensory representation is the total number of APs across the network. Although our previous analysis showed that more neurons are recruited and that firing rates are higher to bimodal stimuli (Figures 3G and 3H), at the network level a suppression of responses could cancel out the increase in spiking in the supra-additive population. To examine this, we first compared unimodal and bimodal network-level spiking responses. We calculated the distribution of the difference between the bimodal and the strongest unimodal response for all units and separated them by sub-population (Figures 6Di–6Div). As expected, the supra-additive population generated additional APs (median: 1.87 ± 1.38 MAD), while the sub-additive population showed a reduction in APs (−1.30 ± 1.71 MAD), and the additive population showed almost no change (−0.13 ± 0.49 MAD). Interestingly, the difference between the sub- and supra-additive medians is small but positive ($\Delta_{medians}$: 0.58 APs), indicating that there is a net-positive effect in network-level spiking during thermotactile stimulation. This effect is observed to a lesser extent in the anesthetized dataset (0.25 APs) and is negative (−0.26 APs) or almost non-existent (0.09 APs) in the warm and light controls, respectively. Although only few additional APs are generated at the network level, these data suggest that a shift in the temporal dynamics leads to a prolongation of the integration window in fS1. We suggest that this is a key property in the cortical representation of thermotactile information.

DISCUSSION

Somatosensation involves a continuous integration of thermal and tactile information. Here, we examined the impact of the integration of cool with tactile information on perception and the neural representation in fS1. We show that cool and touch perception are each enhanced by the addition of the other modality and pinpoint key features of cortical responses including (1) the recruitment of unimodally silent or inhibited neurons, (2) non-linearity of thermotactile responses, and (3) a prolongation of response duration.

Thermotactile perception

To examine the impact of thermotactile integration on detection sensitivity (a change in perceptual threshold) and accuracy (a change in the slope of the psychometric function), we designed a thermotactile Go/No-Go detection task based on an audio-visual integration task for head-fixed mice.[24,37] Prior work suggests that multisensory modulation is enhanced if two stimuli are presented at the same environmental location (spatial congruency), the same time (temporal congruency), and threshold stimulus levels (inverse effectiveness). To achieve spatial congruency, we delivered both stimuli to the right forepaw. However, the touch stimulus was delivered by vibrating the dorsal surface of the forepaw, whereas the thermal stimulus was delivered to the ventral surface. Despite this limitation, both cool and touch stimuli evoked strong and reliable responses in many fS1 neurons, demonstrating overlapping receptive fields. To maintain temporal congruency and mimic the simultaneous timing of cool and touch stimuli during object handling, we delivered both stimuli at the same onset time during thermotactile stimulation. Our task contained multiple amplitudes as well as an adaptive staircase procedure for session-by-session calibration of sensory threshold of both modalities to allow pooling of data across sessions and fitting of psychometric functions.

The data show that mice are more accurate at reporting higher stimulus amplitudes and have low unimodal cool and touch detection thresholds (cool ∼0.5°C, touch ∼2 mN). Moreover, we observed longer reporting latencies to cool (245 ms) than to touch (219 ms) stimuli. It is challenging to compare perceptual features across modalities, but one explanation for this difference could be the differences in neural conduction time for thermal and tactile information to travel from the skin sensory afferent neurons to the cortex (Figure 3D). Cool-sensitive primary sensory afferent neurons are thought to contain a population of slowly conducting C-fibers, as well as a smaller population of faster-conducting, thinly myelinated Aδ-fibers,[38–40] whereas the tactile pathway contains a major population of fast-conducting, myelinated afferent fibers and is optimized for the rapid transfer of information.[41]

The central result from perceptual testing was that the detection of combined thermotactile stimuli was enhanced, compared with unimodal stimuli. This was shown by an increase in the detection rates (Figure 1C) and a reduction in the detection time, compared with unimodal stimuli (Figure 1G). Notably, the difference between maximum unimodal and bimodal detection rates was stronger at threshold stimulus levels than at higher or lower amplitudes (Figure 1I). Further analysis of the psychometric functions showed a significant reduction in threshold during thermotactile stimulation (Figures 1D and 1E), but consistent with prior studies of audio-visual detection,[42,43] there was no overall change in the slope of the psychometric function during thermotactile stimulation (but see Meijer et al.[37]). Therefore, the enhancement of task performance was likely the result of the reduction in perceptual threshold rather than an increase in detection reliability.

Could these results be explained by the mouse being poorly motivated or using limited information in unimodal compared with bimodal testing? This seems unlikely because we observed that the shape of the response time distribution was similar across all conditions (Figure 1F), suggesting similar motivation and use of available sensory information during unimodal and bimodal testing.[5] Instead, we hypothesize that behavioral enhancement results from changes in the cortical neural response features during thermotactile integration.

Cortical representation of thermotactile information

Prior work has shown that mouse fS1 neurons respond to cool and touch stimulation of the forepaw,[28,29] but their thermotactile integration properties had not been investigated. In this study, we attempted to avoid non-sensory input to fS1 and focus on sensory integration properties. We therefore did not combine electrophysiological recordings with behavioral testing. In the future, recordings during a two-alternative forced choice paradigm with delay periods could help dissociate sensory from non-sensory inputs in behaving animals.

Please cite this article in press as: Schnepel et al., Cortical cellular encoding of thermotactile integration, Current Biology (2024), https://doi.org/10.1016/j.cub.2024.03.018

Our data confirm that fS1 neurons show robust responses to unimodal cool and touch and that many neurons encode both modalities (Figure 2D). Similar to the enhanced behavioral reporting of thermotactile stimuli, the cortical response strength was higher for thermotactile than unimodal stimuli (Figure 3B), and responses to tactile stimuli exhibit shorter latencies compared with cool stimuli. However, in contrast to the shorter reporting times for thermotactile stimuli, the neural response latency to thermotactile stimuli fell in between the touch and cool response latencies. A change in behavioral response latency to thermotactile stimuli can therefore not be easily explained by a straightforward correlation between neuronal and behavioral latency. A direct comparison between neuronal and behavioral timescales is challenging due to the integration of information across a population of cells that is larger than is currently possible to record. However, a difference is expected as the average bimodal latency will necessarily be a mix of the two unimodal response latencies. It could also result from the dominance of one modality in the response of a bimodally sensitive unit or indicate that behavioral response latency is a product of one functional subgroup having a more prominent impact on behavior than another. Moreover, while some neurons display very short latencies to strong stimuli (tens of milliseconds), behavioral response latencies increase as the task becomes more difficult (Figure S1B), suggesting that mice accumulate evidence over several hundreds of milliseconds during the sustained response period before making the decision to lick. Overall, in order to further understand the correlation between behavioral and neuronal response timing, recordings during behavior are required. Furthermore, for a more complete understanding, further exploration of different cortical and subcortical regions will be required.

A mechanistic understanding of neuronal features of thermotactile integration will benefit from a combination of different approaches. Recently, for example, Ohshiro and colleagues developed an elegant model that can explain different neuronal response features of multisensory integration through divisive normalization.[44,45] Whether divisive normalization can explain thermotactile cortical responses could now be addressed with a combined recording/modeling approach. Alongside this, future experiments should target subtypes of cortical neurons. For example, the identification of a population of cells showing no change or a reduction in firing rates during unimodal stimulation but large excitatory responses during thermotactile stimulation (e.g., Figure 5B, clusters 2 and 3) suggests an alteration in the level of synaptic inhibition during thermotactile stimulation.[22,46] Future experiments could address this hypothesis with membrane potential recordings from excitatory neurons combined with activity manipulations of cortical GABA-ergic inhibitory interneurons.

A central question regarding cortical multisensory integration is whether stimuli are combined in a linear or non-linear fashion. We found evidence for non-linear supra- and sub- additive responses as well as linear additive neuronal responses (Figures 4 and S5B). Plotting the MSI against the sum of the unimodal responses showed opposing forms of inverse effectiveness for the functional subtypes. As the sum of the unimodal responses decreased, the MSI of supra-additive neurons increased, which would result in a boost of low-saliency inputs. Conversely, the MSI of the sub-additive population decreased, which could be interpreted as a suppression of noisy inputs in an already strongly responding population. Although inverse effectiveness is a well-documented form of non-linear integration and has been proposed as a key mechanism of multisensory integration in several systems,[25,37,47–49] it is not straightforward to assess due to caveats including "ceiling/floor effects" and "regression toward the mean."[50,51] Our stimulation paradigm used an a priori approach that samples responses to a range of defined stimulation intensities, as opposed to sorting neuronal responses by strength. This may mitigate problems associated with regression toward the mean,[51] but issues with noisy estimations of small responses (floor effect) and finite maximum firing rates of neurons (ceiling effect) remain. This makes it difficult to unambiguously identify inverse effectiveness as a mechanism underlying thermotactile enhancement.

We observed a clear difference between the response dynamics of supra-additive, sub-additive, and additive neurons to thermotactile stimulation. Supra-additive neurons showed more sustained responses than sub-additive or additive neurons (e.g., Figures 3A and 4B). A prolongation of responses could favor a more robust representation for hard-to-detect stimuli by increasing the effective integration time window. We also observed that additional APs in the supra-additive population could support prolonged responses (Figure 6). Intriguingly, the subset of neurons with the clearest response prolongation were only weakly responsive or even silent during unimodal stimulation (Figure 5B, clusters 2 and 3), suggesting that they are being recruited during bimodal stimulation (Figures 3G, 3H, and 6Ai–6Ci). Together with the observed delay in response latency to low-saliency unimodal stimuli (Figure S1B), the prolongation of the cortical response could be a substrate for the performance increase during thermotactile perception.

Cortical sensory responses in awake animals can be modulated by arousal, differences in stimulus saliency, and behavioral engagement. To assess the role of arousal, we performed recordings under anesthesia. In contrast to awake data, inverse effectiveness was only observed in the sub-additive population, whereas response prolongation and unit recruitment effects were comparable with those of awake mice (Figures S2 and 6, row ii). Moreover, the prolongation of responses and population level increase in spiking were stronger during cool + touch stimulation compared with warm + touch and light + touch (Figure 6, rows iii–iv), suggesting that these features result from the integration of two modalities of sensory input rather than generalized arousal.

Conclusions and outlook

In conclusion, our behavioral results show that the integration of cool and touch acts to enhance somatosensory perception. They suggest that future studies should consider the temperature of surfaces as a fundamental component of tactile sensation and attempt to dissociate thermal from tactile information.[52] Furthermore, this study establishes mouse fS1 as a model for future investigations into the neural mechanisms of thermotactile integration. The recruitment of additional cortical neurons, nonlinear changes in response strength, and longer response duration are likely key changes in the representation of thermotactile information in fS1, which underlie the enhancement in perception during thermotactile integration. Temporally precise neuronal activity manipulations during thermotactile integration tasks are now required to test this hypothesis.

STAR★METHODS

Detailed methods are provided in the online version of this paper and include the following:

- KEY RESOURCES TABLE
- RESOURCE AVAILABILITY
  - Lead contact
  - Materials availability
  - Data and code availability
- EXPERIMENTAL MODEL AND STUDY PARTICIPANT DETAILS
  - Animals
  - Surgery
- METHOD DETAILS
  - Intrinsic imaging
  - Sensory stimulation
  - Behavioral task
  - Extracellular recordings
  - Histology
  - Extracellular spike sorting
- QUANTIFICATION AND STATISTICAL ANALYSIS
  - Behavioral data analysis
  - Neuronal analysis
  - Statistical tests

SUPPLEMENTAL INFORMATION

Supplemental information can be found online at https://doi.org/10.1016/j.cub.2024.03.018.

ACKNOWLEDGMENTS

This work was supported by the European Research Council (ERC-2015-CoG-682422, J.F.A.P.), the German Research Foundation (DFG, FOR 2143, J.F.A.P.; CRC 1315, J.F.A.P.; and CRC 384, J.F.A.P.), the Boehringer Ingelheim Fonds (BIF, I.E.-R.), Experimental Psychology Society Study Visit (SVO122-03, I.E.-R.), the European Union Horizon 2020 research and innovation programme (grant no. 101017746, P.H.), and the Helmholtz Association (J.F.A.P.). We thank Charlene Memler and Svenja Steinfelder for technical and administrative help.

AUTHOR CONTRIBUTIONS

P.S. and J.F.A.P. designed the study. P.S., I.E.-R., and R.P.-M. performed experiments. P.S. and R.P.-M. analyzed the data. J.F.A.P. and P.H. supervised the project. P.S. and J.F.A.P. wrote the manuscript with input from all authors.

DECLARATION OF INTERESTS

P.S. is currently employed by imec, the Netherlands.

Received: April 2, 2023
Revised: December 24, 2023
Accepted: March 13, 2024
Published: April 5, 2024

REFERENCES

1. Raposo, D., Sheppard, J.P., Schrater, P.R., and Churchland, A.K. (2012). Multisensory decision-making in rats and humans. J. Neurosci. *32*, 3726–3735. https://doi.org/10.1523/JNEUROSCI.4998-11.2012.
2. Gu, Y., Angelaki, D.E., and Deangelis, G.C. (2008). Neural correlates of multisensory cue integration in macaque MSTd. Nat. Neurosci. *11*, 1201–1210. https://doi.org/10.1038/nn.2191.
3. Driver, J., and Noesselt, T. (2008). Multisensory interplay reveals crossmodal influences on 'sensory-specific' brain regions, neural responses, and judgments. Neuron *57*, 11–23. https://doi.org/10.1016/j.neuron.2007.12.013.
4. Godenzini, L., Alwis, D., Guzulaitis, R., Honnuraiah, S., Stuart, G.J., and Palmer, L.M. (2021). Auditory input enhances somatosensory encoding and tactile goal-directed behavior. Nat. Commun. *12*, 4509. https://doi.org/10.1038/s41467-021-24754-w.
5. Nikbakht, N., Tafreshiha, A., Zoccolan, D., and Diamond, M.E. (2018). Supralinear and supramodal integration of visual and tactile signals in rats: psychophysics and neuronal mechanisms. Neuron *97*, 626–639.e8. https://doi.org/10.1016/j.neuron.2018.01.003.
6. Ernst, M.O., and Banks, M.S. (2002). Humans integrate visual and haptic information in a statistically optimal fashion. Nature *415*, 429–433. https://doi.org/10.1038/415429a.
7. Stein, B.E., and Stanford, T.R. (2008). Multisensory integration: current issues from the perspective of the single neuron. Nat. Rev. Neurosci. *9*, 255–266. https://doi.org/10.1038/nrn2331.
8. Marucci, M., Di Flumeri, G., Borghini, G., Sciaraffa, N., Scandola, M., Pavone, E.F., Babiloni, F., Betti, V., and Aricò, P. (2021). The impact of multisensory integration and perceptual load in virtual reality settings on performance, workload and presence. Sci. Rep. *11*, 4831. https://doi.org/10.1038/s41598-021-84196-8.
9. Ferrè, E.R., Walther, L.E., and Haggard, P. (2015). Multisensory interactions between vestibular, visual and somatosensory signals. PLoS ONE *10*, e0124573. https://doi.org/10.1371/journal.pone.0124573.
10. Fetsch, C.R., DeAngelis, G.C., and Angelaki, D.E. (2013). Bridging the gap between theories of sensory cue integration and the physiology of multisensory neurons. Nat. Rev. Neurosci. *14*, 429–442. https://doi.org/10.1038/nrn3503.
11. Meredith, M.A., and Stein, B.E. (1983). Interactions among converging sensory inputs in the superior colliculus. Science *221*, 389–391. https://doi.org/10.1126/science.6867718.
12. Stein, B.E., Magalhaes-Castro, B., and Kruger, L. (1975). Superior colliculus: visuotopic-somatotopic overlap. Science *189*, 224–226. https://doi.org/10.1126/science.1094540.
13. Wallace, M.T., Meredith, M.A., and Stein, B.E. (1998). Multisensory integration in the superior colliculus of the alert cat. J. Neurophysiol. *80*, 1006–1010. https://doi.org/10.1152/jn.1998.80.2.1006.
14. Avillac, M., Ben Hamed, S.B., and Duhamel, J.R. (2007). Multisensory integration in the ventral intraparietal area of the macaque monkey. J. Neurosci. *27*, 1922–1932. https://doi.org/10.1523/JNEUROSCI.2646-06.2007.
15. Benevento, L.A., Fallon, J., Davis, B.J., and Rezak, M. (1977). Auditory–visual interaction in single cells in the cortex of the superior temporal sulcus and the orbital frontal cortex of the macaque monkey. Exp. Neurol. *57*, 849–872. https://doi.org/10.1016/0014-4886(77)90112-1.
16. Graziano, M.S., and Gandhi, S. (2000). Location of the polysensory zone in the precentral gyrus of anesthetized monkeys. Exp. Brain Res. *135*, 259–266. https://doi.org/10.1007/s002210000518.
17. Felleman, D.J., and Van Essen, D.C. (1991). Distributed hierarchical processing in the primate cerebral cortex. Cereb. Cortex *1*, 1–47. https://doi.org/10.1093/cercor/1.1.1-a.
18. Duhamel, J.R., Colby, C.L., and Goldberg, M.E. (1998). Ventral intraparietal area of the macaque: congruent visual and somatic response properties. J. Neurophysiol. *79*, 126–136. https://doi.org/10.1152/jn.1998.79.1.126.
19. Bizley, J.K., Nodal, F.R., Bajo, V.M., Nelken, I., and King, A.J. (2007). Physiological and anatomical evidence for multisensory interactions in auditory cortex. Cereb. Cortex *17*, 2172–2189. https://doi.org/10.1093/cercor/bhl128.

20. Ghazanfar, A.A., and Schroeder, C.E. (2006). Is neocortex essentially multisensory? Trends Cogn. Sci. *10*, 278–285. https://doi.org/10.1016/j.tics.2006.04.008.

21. Morrell, F. (1972). Visual system's view of acoustic space. Nature *238*, 44–46. https://doi.org/10.1038/238044a0.

22. Iurilli, G., Ghezzi, D., Olcese, U., Lassi, G., Nazzaro, C., Tonini, R., Tucci, V., Benfenati, F., and Medini, P. (2012). Sound-driven synaptic inhibition in primary visual cortex. Neuron *73*, 814–828. https://doi.org/10.1016/j.neuron.2011.12.026.

23. Fishman, M.C., and Michael, P. (1973). Integration of auditory information in the cat's visual cortex. Vision Res. *13*, 1415–1419. https://doi.org/10.1016/0042-6989(73)90002-3.

24. Meijer, G.T., Marchesi, P., Mejias, J.F., Montijn, J.S., Lansink, C.S., and Pennartz, C.M.A. (2020). Neural correlates of multisensory detection behavior: comparison of primary and higher-order visual cortex. Cell Rep. *31*, 107636. https://doi.org/10.1016/j.celrep.2020.107636.

25. Lakatos, P., Chen, C.M., O'Connell, M.N., Mills, A., and Schroeder, C.E. (2007). Neuronal oscillations and multisensory interaction in primary auditory cortex. Neuron *53*, 279–292. https://doi.org/10.1016/j.neuron.2006.12.011.

26. Wallace, M.T., Ramachandran, R., and Stein, B.E. (2004). A revised view of sensory cortical parcellation. Proc. Natl. Acad. Sci. USA *101*, 2167–2172. https://doi.org/10.1073/pnas.0305697101.

27. Bimbard, C., Sit, T.P.H., Lebedeva, A., Reddy, C.B., Harris, K.D., and Carandini, M. (2023). Behavioral origin of sound-evoked activity in mouse visual cortex. Nat. Neurosci. *26*, 251–258. https://doi.org/10.1038/s41593-022-01227-x.

28. Milenkovic, N., Zhao, W.J., Walcher, J., Albert, T., Siemens, J., Lewin, G.R., and Poulet, J.F.A. (2014). A somatosensory circuit for cooling perception in mice. Nat. Neurosci. *17*, 1560–1566. https://doi.org/10.1038/nn.3828.

29. Vestergaard, M., Carta, M., Güney, G., and Poulet, J.F.A. (2023). The cellular coding of temperature in the mammalian cortex. Nature *614*, 725–731. https://doi.org/10.1038/s41586-023-05705-5.

30. Filingeri, D. (2016). Neurophysiology of skin thermal sensations. In Comprehensive Physiology, *Vol. 6*, R. Terjung, ed. (Wiley), p. 1429.

31. Murray, D.J., and Ross, H.E. (1996). E.H. Weber on the Tactile Senses, First Edition (Routledge).

32. Green, B.G. (1977). Localization of thermal sensation: an illusion and synthetic heat. Percept. Psychophys. *22*, 331–337. https://doi.org/10.3758/BF03199698.

33. Cataldo, A., Ferrè, E.R., di Pellegrino, G., and Haggard, P. (2016). Thermal referral: evidence for a thermoceptive uniformity illusion without touch. Sci. Rep. *6*, 35286. https://doi.org/10.1038/srep35286.

34. Ho, H.N., Watanabe, J., Ando, H., and Kashino, M. (2011). Mechanisms underlying referral of thermal sensations to sites of tactile stimulation. J. Neurosci. *31*, 208–213. https://doi.org/10.1523/JNEUROSCI.2640-10.2011.

35. Paricio-Montesinos, R., Schwaller, F., Udhayachandran, A., Rau, F., Walcher, J., Evangelista, R., Vriens, J., Voets, T., Poulet, J.F.A., and Lewin, G.R. (2020). The sensory coding of warm perception. Neuron *106*, 830–841.e3. https://doi.org/10.1016/j.neuron.2020.02.035.

36. Prsa, M., Kilicel, D., Nourizonoz, A., Lee, K.S., and Huber, D. (2021). A common computational principle for vibrotactile pitch perception in mouse and human. Nat. Commun. *12*, 5336. https://doi.org/10.1038/s41467-021-25476-9.

37. Meijer, G.T., Pie, J.L., Dolman, T.L., Pennartz, C.M.A., and Lansink, C.S. (2018). Audiovisual integration enhances stimulus detection performance in mice. Front. Behav. Neurosci. *12*, 231. https://doi.org/10.3389/fnbeh.2018.00231.

38. Mackenzie, R.A., Burke, D., Skuse, N.F., and Lethlean, A.K. (1975). Fibre function and perception during cutaneous nerve block. J. Neurol. Neurosurg. Psychiatry *38*, 865–873. https://doi.org/10.1136/jnnp.38.9.865.

39. Darian-Smith, I., Johnson, K.O., and Dykes, R. (1973). "Cold" fiber population innervating palmar and digital skin of the monkey: responses to cooling pulses. J. Neurophysiol. *36*, 325–346. https://doi.org/10.1152/jn.1973.36.2.325.

40. Campero, M., Serra, J., Bostock, H., and Ochoa, J.L. (2001). Slowly conducting afferents activated by innocuous low temperature in human skin. J. Physiol. *535*, 855–865. https://doi.org/10.1111/j.1469-7793.2001.t01-1-00855.x.

41. Abraira, V.E., and Ginty, D.D. (2013). The sensory neurons of touch. Neuron *79*, 618–639. https://doi.org/10.1016/j.neuron.2013.07.051.

42. Lippert, M., Logothetis, N.K., and Kayser, C. (2007). Improvement of visual contrast detection by a simultaneous sound. Brain Res. *1173*, 102–109. https://doi.org/10.1016/j.brainres.2007.07.050.

43. Hollensteiner, K.J., Pieper, F., Engler, G., König, P., and Engel, A.K. (2015). Crossmodal integration improves sensory detection thresholds in the ferret. PLoS ONE *10*, e0124952. https://doi.org/10.1371/journal.pone.0124952.

44. Ohshiro, T., Angelaki, D.E., and DeAngelis, G.C. (2011). A normalization model of multisensory integration. Nat. Neurosci. *14*, 775–782. https://doi.org/10.1038/nn.2815.

45. Ohshiro, T., Angelaki, D.E., and DeAngelis, G.C. (2017). A neural signature of divisive normalization at the level of multisensory integration in primate cortex. Neuron *95*, 399–411.e8. https://doi.org/10.1016/j.neuron.2017.06.043.

46. Olcese, U., Iurilli, G., and Medini, P. (2013). Cellular and synaptic architecture of multisensory integration in the mouse neocortex. Neuron *79*, 579–593. https://doi.org/10.1016/j.neuron.2013.06.010.

47. Alvarado, J.C., Stanford, T.R., Vaughan, J.W., and Stein, B.E. (2007). Cortex mediates multisensory but not unisensory integration in superior colliculus. J. Neurosci. *27*, 12775–12786. https://doi.org/10.1523/JNEUROSCI.3524-07.2007.

48. Meredith, M.A., and Stein, B.E. (1986). Visual, auditory, and somatosensory convergence on cells in superior colliculus results in multisensory integration. J. Neurophysiol. *56*, 640–662. https://doi.org/10.1152/jn.1986.56.3.640.

49. van de Rijt, L.P.H., Roye, A., Mylanus, E.A.M., van Opstal, A.J., and van Wanrooij, M.M. (2019). The principle of inverse effectiveness in audiovisual speech perception. Front. Hum. Neurosci. *13*, 335. https://doi.org/10.3389/fnhum.2019.00335.

50. Holmes, N.P. (2007). The law of inverse effectiveness in neurons and behaviour: multisensory integration versus normal variability. Neuropsychologia *45*, 3340–3345. https://doi.org/10.1016/j.neuropsychologia.2007.05.025.

51. Holmes, N.P. (2009). The principle of inverse effectiveness in multisensory integration: some statistical considerations. Brain Topogr. *21*, 168–176. https://doi.org/10.1007/s10548-009-0097-2.

52. Ezquerra-Romano, I., Chowdhury, M., Leone, C.M., Iannetti, G.D., and Haggard, P. (2023). A novel method to selectively elicit cold sensations without touch. J. Neurosci. Methods *385*, 109763. https://doi.org/10.1016/j.jneumeth.2022.109763.

53. Prins, N., and Kingdom, F.A.A. (2018). Applying the model-comparison approach to test specific research hypotheses in psychophysical research using the Palamedes Toolbox. Front. Psychol. *9*, 1250. https://doi.org/10.3389/fpsyg.2018.01250.

54. Brainard, D.H. (1997). The Psychophysics Toolbox. Spat. Vis. *10*, 433–436. https://doi.org/10.1163/156856897X00357.

55. Pachitariu, M., Stringer, C., Dipoppa, M., Schröder, S., Rossi, L.F., Dalgleish, H., Carandini, M., and Harris, K.D. (2017). Suite2p: beyond 10,000 neurons with standard two-photon microscopy. Preprint at bioRxiv. https://doi.org/10.1101/061507.

56. Berditchevskaia, A., Cazé, R.D., and Schultz, S.R. (2016). Performance in a GO/NOGO perceptual task reflects a balance between impulsive and instrumental components of behaviour. Sci. Rep. *6*, 27389. https://doi.org/10.1038/srep27389.

57. Shamash, P., Carandini, M., Harris, K.D., and Steinmetz, N.A. (2018). A tool for analyzing electrode tracks from slice histology. Preprint at bioRxiv. https://doi.org/10.1101/447995.

58. Antoine, M.W., Langberg, T., Schnepel, P., and Feldman, D.E. (2019). Increased excitation-inhibition ratio stabilizes synapse and circuit excitability in four autism mouse models. Neuron *101*, 648–661.e4. https://doi.org/10.1016/j.neuron.2018.12.026.

59. Shimazaki, H., and Shinomoto, S. (2007). A method for selecting the bin size of a time histogram. Neural Comput. *19*, 1503–1527. https://doi.org/10.1162/neco.2007.19.6.1503.

Please cite this article in press as: Schnepel et al., Cortical cellular encoding of thermotactile integration, Current Biology (2024), https://doi.org/10.1016/j.cub.2024.03.018

STAR★METHODS

KEY RESOURCES TABLE

REAGENT or RESOURCE	SOURCE	IDENTIFIER
Deposited data		
Dataset and MATLAB code	This study	Zenodo: https://zenodo.org/doi/10.5281/zenodo.10783617
Experimental models: Organisms/strains		
Mouse C57BL6	MDC animal facility	N/A
Software and algorithms		
MATLAB 2017a	MathWorks	https://www.mathworks.com/
Palamedes Toolbox v1.10.8	Prins and Kingdom[53]	https://www.palamedestoolbox.org/
Psychophysics Toolbox 3	Brainard[54]	http://psychtoolbox.org/
Spikes	Steinmetz	https://github.com/cortex-lab/spikes
Kilosort 2.0	Pachitariu et al.[55]	https://github.com/MouseLand/Kilosort

RESOURCE AVAILABILITY

Lead contact

Further information and requests for resources and reagents should be directed to and will be fulfilled by the lead contact, James Poulet (james.poulet@mdc-berlin.de).

Materials availability

This study did not generate new unique reagents.

Data and code availability

- All data reported in this study will be shared by the lead contact upon request.
- All original code has been deposited at zenodo.org and is publicly available as of the date of publication. DOIs are listed in the key resources table.
- Any additional information required to reanalyze the data reported in this study is available from the lead contact upon request.

EXPERIMENTAL MODEL AND STUDY PARTICIPANT DETAILS

Animals

All experiments were conducted according to European law and the state of Berlin animal welfare body (LAGeSo). Male C57BL/6J mice between P52 - P198 (median: P68) were used and maintained on a 12:12 hr light-dark cycle. Experiments were performed during the light phase. Mice were gradually habituated to head and paw fixation.

Surgery

Mice were deeply anesthetized using 3-4 % isoflurane in 100 % O_2 (maintained at 1.5-2 % isoflurane) and injected with metamizol (200 mg / kg) and 0.3-0.5ml warm sterile saline solution to avoid post-operative pain and ensure hydration. Mice were fixed in a stereotactic frame (SR-9AH, Narishige, Tokyo, Japan) using ear bars, eye gel (Vidisic, Bausch+Lomb, Laval, Canada) was applied and body temperature was maintained using a heating pad and rectal probe (50300, Stoelting, Wood Dale IL, USA). Custom-made head holders were attached to the cleaned skull and a well was build using dental cement and covered with KwikCast (World Precision Instruments, Sarasota FL, USA). After surgery, mice were kept on the warm heating pad until they awoke from anesthesia. Metamizol was dissolved in the drinking water for minimum of 48 hr to avoid post-operative pain.

METHOD DETAILS

Intrinsic imaging

Intrinsic signal optical imaging (ISOI) was used to identify the location of fS1 for electrophysiological recordings. On the day of recording, mice were deeply anesthetized and then maintained at light anesthesia levels (1-1.5 % isoflurane) for ISOI. The forepaw was stimulated with a 100 Hz sinusoidal vibration for 5 s using a Piezo element (PL127.11, Physik Instrumente, Karlsruhe, Germany),

Please cite this article in press as: Schnepel et al., Cortical cellular encoding of thermotactile integration, Current Biology (2024), https://doi.org/10.1016/j.cub.2024.03.018

image frames were captured with a CMOS camera (QICAM Fast 1394, Teledyne, Surrey, Canada) and analyzed online using custom software written in Igor (WaveMetrics, Lake Oswego OR, USA) or MATLAB (Mathworks, Natick CA, USA). Once a robust response was detected, a craniotomy was performed over the area and 1 or 2 incisions were made in the dura to facilitate probe insertion. For recovery from surgery prior to awake recordings, the craniotomy was covered with a drop of Ringer's and the well was sealed with KwikCast. The animal was allowed to wake up and recover from anesthesia for at least 1h before starting the extracellular recording procedure.

Sensory stimulation

Stimulus presentation was controlled via custom-written MATLAB-scripts and a DAQ-board (NI-6232, National Instruments, Austin TX, USA) and synchronized with the recording setup (see below) via TTL pulses. Additionally for the behavior experiments (see below), the trial structure and real-time feedback was controlled with a state machine (bpod, Sanworks, Rochester NY, USA). Touch stimuli were delivered via a force-feedback lever system (300C, Aurora Scientific, Aurora ON, Canada) as a sinusoidal vibration to the top of the paw for 1 s at 60 Hz at different intensities. The force at the tip of the lever was recorded to detect movement of the animal during the recording and to implement an online feedback correction to keep the stimulus intensity consistent across trials in case the animal slightly moved the paw against the tape fixation. Temperature stimuli were delivered via 5 high-performance 3.2 x 2.4 mm Peltier elements (TCSII, QST Labs, Strasbourg, France) covering the whole paw of the animal. The stimulus consisted of a ramp-hold-return (1 s duration for behavior and 3 s duration for electrophysiological recordings) at a ramp speed of 300 °C / s covering a range of +/-8 °C from baseline (32 °C) at a resolution of 0.1 °C. Visual stimuli were delivered via a white LED positioned ~8 cm from the contralateral eye mimicking the ramp-hold-return temperature stimulus at intensities of 12.5, 25, 50 and 100 cd/m^2 (calibrated using ColorCAL MkII, Cambridge Research Systems, UK). In a subset of experiments, a second Neuropixels probe was inserted into primary visual cortex (V1) to ensure that the visual stimulation evoked neuronal responses (data not shown).

Behavioral task

The thermotactile Go / NoGo detection task structure and analysis were based on Meijer et al.[37] Animals (n = 8) were trained in several steps to detect both cool (C) and touch (T) stimuli until they surpassed a d' criterion of 1.5 for each step: 1) stimulus pairing with reward 2) blocks of training to detect C or T stimuli only 3) C and T interleaved. We did not reward correct rejections and false alarms were not punished, however if mice licked prior to the stimulus, the next trial was delayed acting as a 'time out'. Psychometric curves for both modalities were generated using an adaptive staircase method in the Go/NoGo task (PsychStairCase of the Psychophysics Toolbox for MATLAB[54]) (Figure S1A). Bimodal stimulus trials were realized by combining the last used unimodal stimulus intensities from each staircase. All trials were pseudo-randomly interleaved (not more than 4x the same modality in a row). Animals performed on average 1959 trials (range: 1138-2944) over 5-11 sessions. Animals performing Go/NoGo tasks, can devise alternative response strategies to obtain rewards even at low performance levels or become over-motivated and generate false positives.[56] We therefore excluded periods where the FA-rate was above 20 % and used randomized periods (ITI 3-7 s + 4-5 s timeout) after each trial to discourage the animals from developing stereotypical licking patterns. Periods where the false alarm (FA) rate stayed on average over 20% were identified using a 100 trials wide sliding window and excluded from analysis. This allowed pooling of data from different mice with similar behavioral motivation levels and resulted in the exclusion of 12.8% of all trials across all mice.

Extracellular recordings

All recordings were performed with Neuropixels 1.0 probes (imec, Leuven, Belgium) and the spikeGLX acquisition package (Bill Karsh, Janelia Research Campus, Ashburn VA, USA) via a PXI interface (NI-PXIe-1071, National Instruments, Austin TX, USA). Probes were coated with DiI (Invitrogen, Waltham MA, USA) and lowered into the tissue automatically via micromanipulators (LN25, Luigs&Neumann, Ratingen, Germany) to a recording depth of 1500-1800 μm at a speed of ~2 μm / s. Raw data was acquired at ~30 kHz (actual rate calibrated for each probe separately) from up to 384 electrodes.

Histology

After the recording, mice were decapitated under deep anesthesia and the brain was immersed in paraformaldehyde (PFA) for minimum of 24 hr. 100 μm thick slices were cut on a vibratome (VT12000S, Leica, Wetzlar, Germany) and imaged on a fluorescence microscope (AxioImager.M2, Karl Zeiss Microscopy GmbH, Göttingen, Germany) to visualize the DiI probe track. Slice images were subsequently transformed and aligned to the Allen Institute mouse brain atlas using the SHARP-track package[57] to confirm the location of the recording in fS1.

Extracellular spike sorting

Spike sorting was performed offline using Kilosort 2.0.[55] Manual curation of the sorted units was performed using the Phy2 package (https://github.com/cortex-lab/phy). Splitting and merging of clusters was kept to a minimum and manual curation was mostly used to tag putative single units and exclude drifting units and artifacts for subsequent analysis. After manual curation, all remaining units were evaluated by 3 main quality metrics: minimum number of spikes > 1000, refractory period (1.5 ms) violations < 0.5%, number of missing spikes < 10% (evaluated as the overlap of 2 gaussian fits to the waveform and noise amplitude distributions).

Please cite this article in press as: Schnepel et al., Cortical cellular encoding of thermotactile integration, Current Biology (2024), https://doi.org/10.1016/j.cub.2024.03.018

QUANTIFICATION AND STATISTICAL ANALYSIS

Behavioral data analysis

Behavior data was analyzed using the Palamedes Toolbox.[53] In short, maximum likelihood fitting with a Weibull function with 3 free (FA-rate, threshold, slope) and 1 fixed parameter (lapse rate) was used to estimate the psychometric functions for each condition. Lapse and FA rates were determined from blank and maximum intensity trials, respectively. Significant changes in threshold and slope between conditions were determined by comparing the transformed likelihood ratios of the full model to a model where either slope or threshold were fixed. The bimodal psychometric data ($cool_{touch}$ / $touch_{cool}$) was created by using all bimodal trials where the 'other' modality's intensity was subthreshold with respect to its unimodal psychometric curve. Subjective intensity was calculated by binning trials according to their stimulus intensity into an equal 5 x 5 grid and then calculating a weighted average of the detection rate across mice according to the number of trials in each bin per mouse. Enhancement was calculated as the % difference between the multimodal and best (i.e. highest) unimodal response rate for a given bin (Figure 1I).

Neuronal analysis

Offline analysis of stimulus responses was performed for each putative single unit using custom MATLAB scripts and existing code (https://github.com/cortex-lab/spikes). Responses were defined as the average, baseline-corrected firing rate (or z-score) in response windows of varying size (default: 1 s) after stimulus onset. The stimulus space consisted of 4 x 5 = 20 amplitude combinations for touch and temperature (0, 5, 10, 20 mN and 0, ±1, ±2, ±4, ±8 °C) with 25 repetitions per stimulus. Units were considered 'responsive' to a particular stimulus if the number of APs measured in the response window deviated significantly from the spiking probability of a Poisson process with that unit's mean baseline firing rate by using a 'binless' method (i.e. using bins of 1ms, $\alpha < 0.01$, [58]). The first bin to cross the significance threshold of $\alpha < 0.01$ was used as the latency of this unit's response. Units were determined as 'overall responsive' if at least 2+x out of 20 stimuli elicited significant responses with x being the rounded false positive detection rate (fpr) of the binless method determined from blank trials multiplied by 20 (average over 22 awake recordings: fpr = 0.0512 ± 0.0047; average over 6 anesthetized recordings: fpr = 0.1022 ± 0.0291).

PSTHs were constructed using an optimal bin size algorithm.[59] Instantaneous firing rate was calculated using a gaussian KDE. Hierarchical clustering was performed on the z-scored KDE over the whole trial of a particular stimulus combination (maximum unimodal stimulus intensities (20 mN / -8°C) for 2 x 2 clustering; 'best' stimulus combination from additivity analysis for 3 x 3 clustering, see below) for each unit using the 'linkage' and 'cluster' functions in MATLAB.

The additivity of each unit was determined as follows: First, for each possible stimulus combination, the distribution of the arithmetic sum of the unimodal response values was bootstrapped (10000 iterations, 12 stimulus combinations) and then z-scored. If the z-score of the actual bimodal response surpassed ± 1.96, this response was considered supra- or sub-additive, respectively and additive otherwise). The stimulus combination which had the maximum absolute z-score was tagged as the 'best' combination. To investigate the best stimulus combinations further, we went on to plot the distribution of stimulus intensities for the best combinations separately for each modality (Figure S4B). While the majority of best combinations contain maximum intensity unimodal stimuli, the supra-additive population exhibits more lower intensity combinations than the sub-additive population. The Multisensory Index was calculated as the difference between the bimodal and the summed unimodal responses normalized by the sum of both (MSI = M - (T + C) / M + (T + C)).

Statistical tests

Statistical tests were performed using MATLAB built-in functions. Normality of the data was tested using the Jarque-Bera test and the following parametric or non-parametric test were used: Between two conditions: t-test / Wilcoxon ranksum; Across several conditions: 1-way ANOVA / Kruskal-Wallis for multiple comparisons with Dunn-Sidak correction. If not otherwise noted, values are reported as mean ± S.E.M. (standard error of the mean). p-values denoted by asterisks: ***: $p < 0.001$, **: $p < 0.01$, *: $p < 0.5$, n.s.: not significant.

Current Biology, Volume *34*

Supplemental Information

Cortical cellular encoding of thermotactile integration

Philipp Schnepel, Ricardo Paricio-Montesinos, Ivan Ezquerra-Romano, Patrick Haggard, and James F.A. Poulet

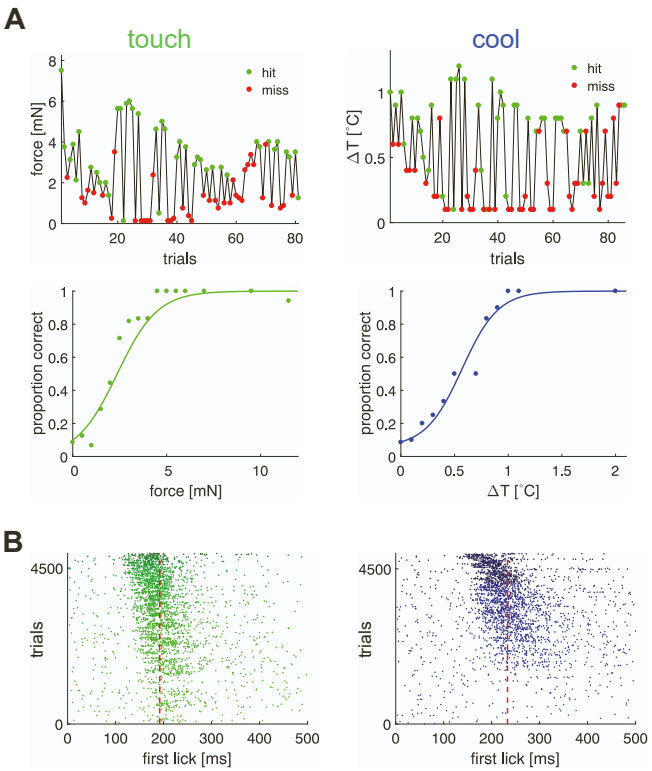

Figure S1. Staircase stimulation procedure during behavioral testing and behavioral latency related to Figure 1

(**A**) Top shows behavioral results from stimulus staircase procedure for an example session from one mouse for both touch and cool stimuli; bottom shows corresponding psychometric curve fit. (**B**) Raster plots showing lick timing across trials for all mice for touch (left) and cool (right) unimodal stimuli. Plots are ordered by stimulus intensity (top strong to bottom weak) and show longer latency for weaker stimuli. Red dotted line denotes median first lick latency.

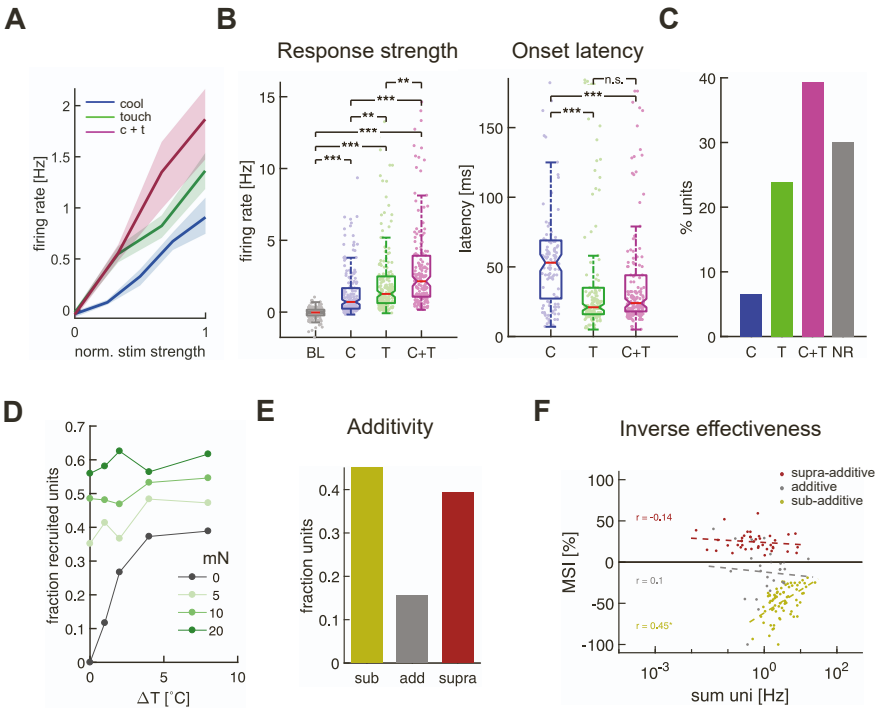

Figure S2. Recruitment and additivity during thermotactile integration are preserved under isoflurane anesthesia, related to Figures 3 and 4

(**A**) Average firing rate of all responsive units to increasing stimulus intensity for touch (T), cool (C) and cool+touch (C+T) stimulation. (**B**) Median response strength (left) and onset latency (right) for all responsive units for all stimulus conditions (BL = baseline). Significant differences were determined by multiple comparison testing (Kruskal-Wallis test). (**C**) Fractions of responsive and unresponsive single units (n = 259 total) at maximum intensity stimulation. (**D**) The fraction of recruited units as a function of stimulus intensity. (**E**) Fractions of units in different sub-populations show that most units are either sub- or supra-additive.(**F**) MSI plotted against the arithmetic sum of the corresponding unimodal stimulus response. Inverse effectiveness is estimated by linear fits to the different sub-populations of neurons (r = 0.3, p = 0.14; r = -0.14, p = 0.37; r = 0.45, p = 0.0001 for the additive and supra-/sub-additive populations, respectively).

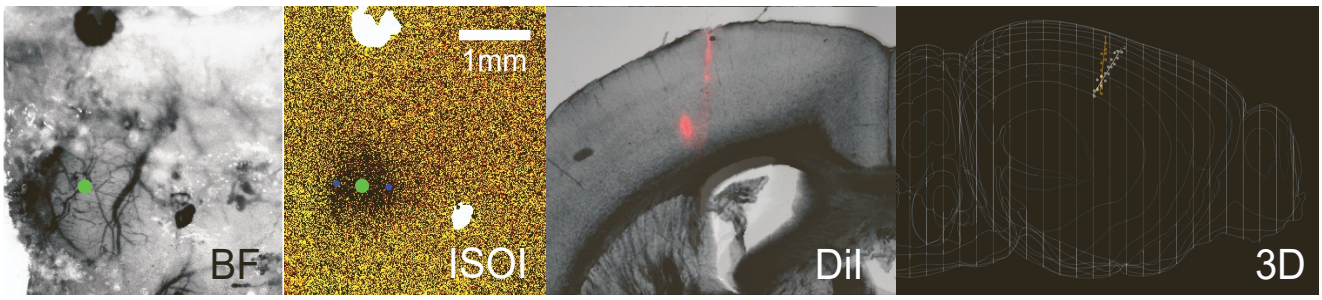

Figure S3. Identification of forepaw S1 an tracking of recording electrode location in an example mouse, related to Figure 2

Panels from left to right: Craniotomy under brightfield (BF) illumination; corresponding intrinsic signal optical imaging (ISOI). Darker area denotes response to tactile stimulation of the forepaw. Green dot denotes the same spot in both panels. (iii) DiI-staining in a horizontal brain slice (100 µm thickness) of two Neuropixel probe tracts and (iv) 3-D reconstruction of both probe trajectories in a normalized mouse brain model (SHARP-track / Allen mouse brain atlas).

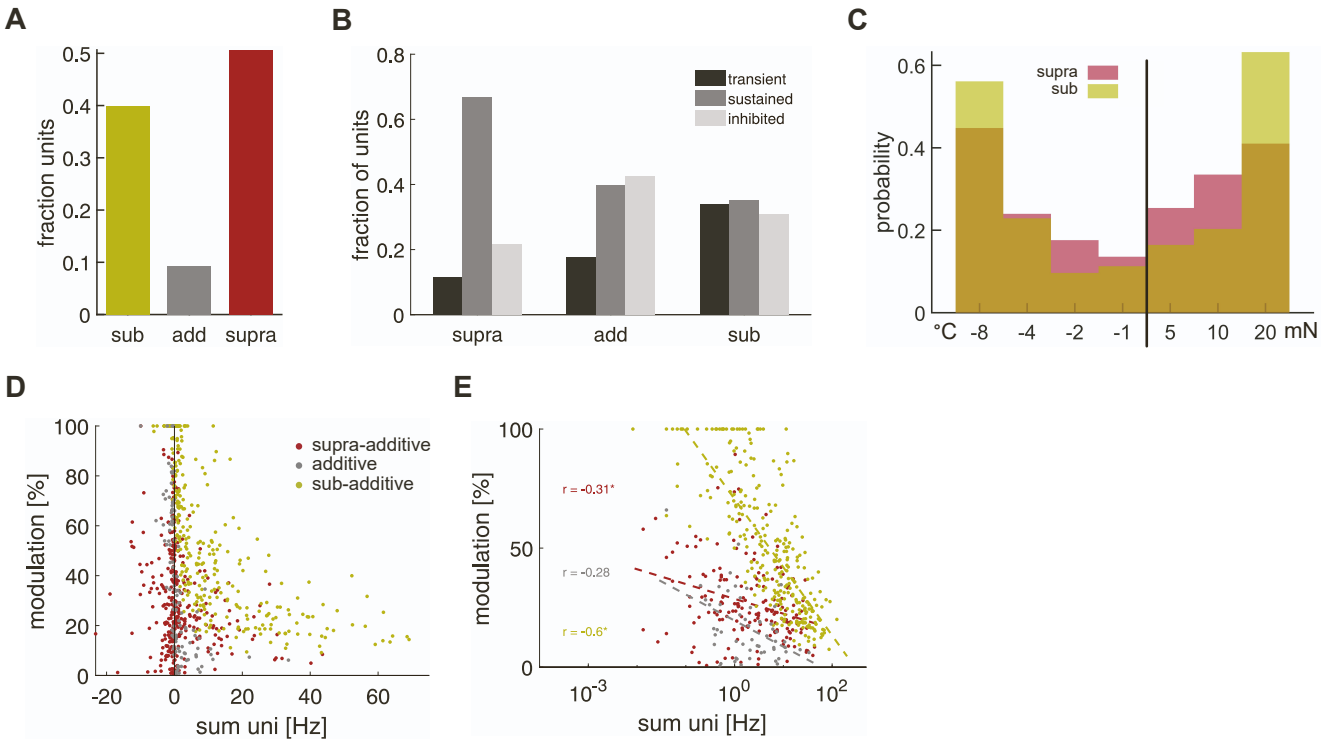

Figure S4. Comparison of additivity sub-populations and absolution response modulation for inverse effectiveness, related to Figure 4

(**A**) Fraction of excited units in respective sub-populations after additivity analysis. (**B**) Fraction of units that showed transient, sustained or suppressed response dynamics in each sub-population. (**C**) Distributions of stimulus combinations that produce 'best' responses during bimodal stimulation for the sub-additive (yellow) and supra-additive (red) population. (**D**) Absolute modulation (normalized quantification of bimodal enhancement/suppression) plotted against the arithmetic sum of the corresponding unimodal stimulus responses. (**E**) Same as in D but on a semi-log scale. A linear regression of the data reveals a significant negative correlation (i.e. inverse effectiveness) for both sub- and supra-additive populations, but not for the additive population.

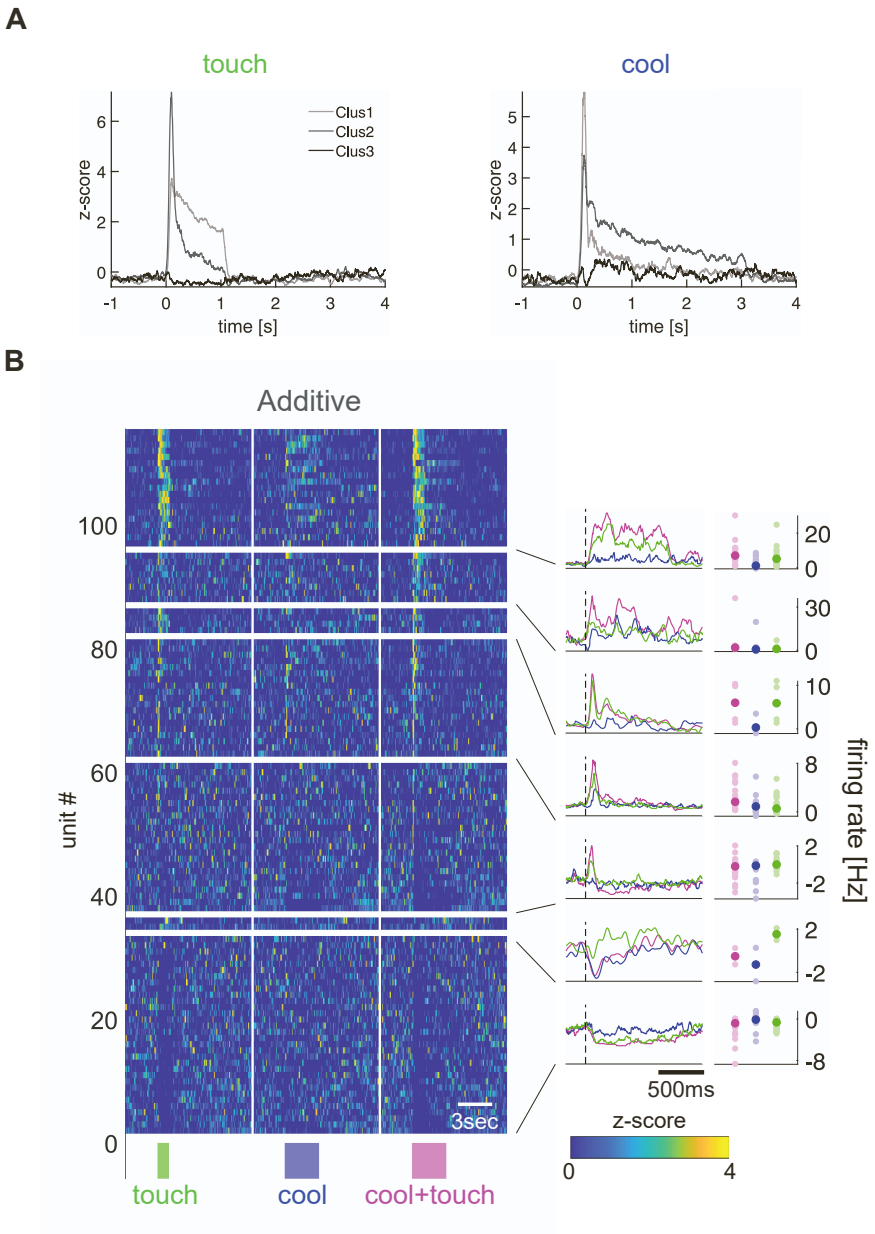

Figure S5. Temporal dynamics and clustering of the additive sub-population, related to Figure 5

(**A**) Average z-scored responses of sub-clusters after hierarchical 3-by-3 clustering for touch (left) and cool (right). (**B**) Hierarchical 3-by-3 clustering of 'best' bimodal responses of the additive sub-population. Each row shows the concatenated, z-scored responses to touch (left), cool (middle) and cool+touch (right) stimulation for each unit. Clusters are ordered by temporal dynamics of the average cool+touch response (left side panels) from sustained over transient to no inhibited/ unresponsive. Within each cluster, units are ordered by peak response strength in the cool+touch condition. Right side panels show the median responses from 0-1200ms of each cluster. There were no significant differences between conditions.

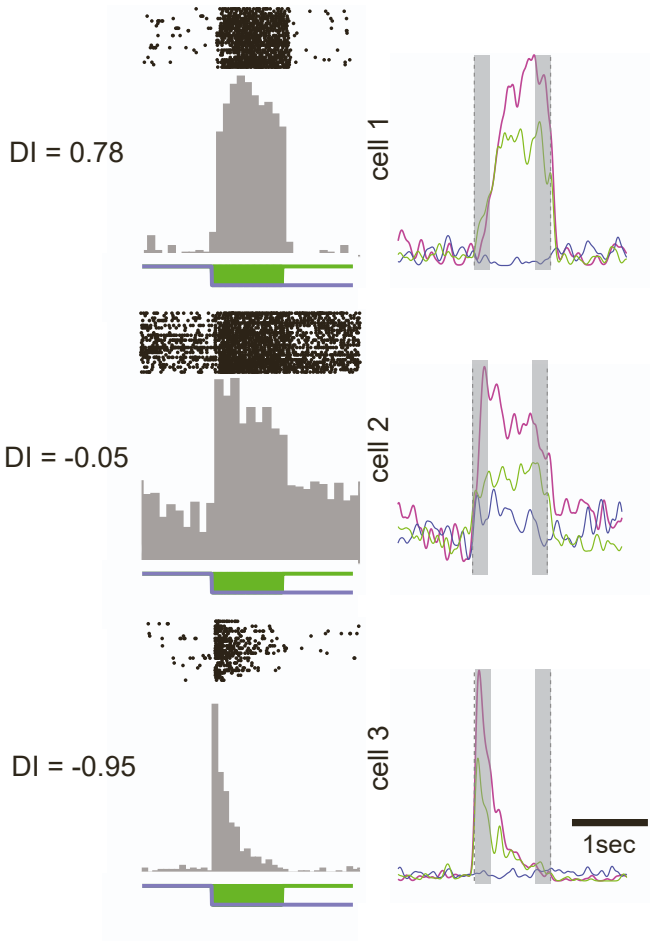

Figure S6. Example units with different duration indices, related to Figure 6

Left, PSTHs and raster plots for example units with different duration indices (DI). Right, early and late response phases for the same cells are marked with gray bars in the KDE-plots.